5 Finite element analysis

5.1 Introduction

Modeling and analysis of composite slabs using the finite element (FE) method has been the subject of much research. However, since the publication of FE based research by Veljkovic (1994, 1995), it is apparent that the commonly used method of applying the non-variable *shear bond-slip relationship* (herein also called *shear interaction property*) obtained from elemental push tests will not produce satisfactory results if they are not modified in accordance with the response and behavior of the slabs. This chapter deals with modeling composite slabs using FE method with a focus on the effect of variable shear interaction property on the result of the analysis.

5.2 Objective

The primary objective of this part of the study is to demonstrate that the small scale bending test can be used to generate a shear bond stress-slip relationship for use in the finite element (FE) analysis. The second objective is to show that the magnitude of the interaction property between the concrete and steel deck is influenced considerably by the slenderness of the slab. The author believes that the use of a non variable interaction property curve, which is typically obtained from elemental push tests in which slenderness and bending behavior are absent, does not provide generally accurate FE results. This is especially true for models with values of slab slenderness that vary from the push tests.

In the following sections, composite slab analysis using the FE method is first reviewed. Then the development of the FE model applied in this work is presented. Next, the use of the shear interaction property obtained from small scale tests is demonstrated, and lastly the results for FE analysis on models with variable geometries are shown.

5.3 Review of the FE method in composite slabs

Daniels and Crisinel (1993a, 1993b) developed a special purpose FE procedure using plane beam elements for analyzing single and continuous span composite slabs. The procedure incorporated nonlinear behavior of material properties, additional positive moment reinforcement, the load-slip property for shear studs (obtained from push tests commonly used for welded shear studs), and the shear interaction property between the concrete and the steel deck (obtained from pull out test developed by the authors, see Sec. 2.3.5). A ductile load-carrying mechanism was employed in the model, neglecting the brittle portion of the push test data. The compressive stress-strain behavior of the deck was specified differently from the tensile behavior where the relationship was estimated from flexural tests on bare deck. In their study, the maximum load capacities for models with different span lengths were shown to lie along the straight line if plotted on the *m-k* axes (see the *m-k* method in Sec. 4.4) but fell outside the same straight line if the steel thickness is changed. The authors attributed this result to the distribution of the shear stress which depended less on span length than it did on slab thickness.

An (1993) studied the behavior of composite slabs with 2D nonlinear FE using the ABAQUS/Standard module. The steel sheeting and the concrete were modeled as 2-node Timoshenko beam elements. The interaction between the steel sheeting and the concrete slab was modeled with spring elements plus a set of imposed equations between degrees of

freedom of concrete, spring and steel deck beam elements. The spring property was obtained from a block bending test (see Sec. 2.6.8). A smeared crack model was used for concrete cracking, while a nonlinear stress-strain curve was used for the steel deck and concrete in compression. The force slip relationship to simulate separation behavior between concrete and steel deck in the vertical direction was assumed as linear elastic and was also modeled with spring elements. The FE results were found to be in good agreement with full scale tests for long slabs but underestimated the capacity of the short slabs. The author reasoned that the underestimation was due to exclusion of the effect of the reaction force in the FE model. Analysis conducted with different vertical separation properties did not produce variable results.

Veljkovic (1996a) performed 3D FE using DIANA to study the mechanics of the force transfer from the sheeting to the concrete in composite slabs. Based on tensile tests of embossed and flat parts of the sheeting, different uniaxial stress-strain relationships were used for the web and the flange. Shear interaction between the sheeting and the concrete was modeled using a nodal interface element and the property was obtained from push tests (Sec. 2.3.9). The interface property was modified with a reduction function (further discussion is given in Sec. 5.7). This was done because the shear interface property was found to decrease with increasing strain in the steel sheeting. The reduction function was obtained from push-pull tests where the steel sheeting was put under tensile strain while the concrete was pushed over it. The steel strain reduced the resistance of the embossment interlock and may more closely represent the behavior occurring in real slabs. A similar modeling method was also reported in Wright and Veljkovic (1996).

Widjaja (1997) performed FE analysis of composite slabs based on a similar model used by An (1993). Slabs with shear stud and weld anchorage at the supports were analyzed. The force-slip relationship for the interface element was obtained from elemental tests similar to that used by Daniels (1988) and the end anchorage was obtained from a modified composite beam push off test. The vertical force-slip relationship was neglected. The results of the analysis were found to be in good agreement with the full scale test results. Result pertaining to variable geometries was not reported.

5.4 Development of the FE model

Three-dimensional nonlinear FE modeling and analysis of composite slabs was carried out in this study using ABAQUS/Explicit 6.3. The input via a text-based file was chosen instead of the interactive method (ABAQUS/CAE) because the text file format was short, self-explanatory and presentable in this report.

In the preliminary development of the FE model, several material properties, particularly the concrete cracking parameters and nonlinearity of the steel sheeting, were tried to determine a suitable combination that produced acceptable results. The initial values of the material properties were chosen based on several reported studies (Abaqus, 2002; Alfaiate et al., 1997; Hillerborg et al., 1976; Veljkovic, 1996a). Top flange buckling was observed in the test (Fig. 3.3(b)) and it dictated the behavior beyond ultimate load. However the model used in this study did not include the buckling of the top flange of the steel sheeting. In this study the compression and tension property for the steel sheeting were assumed the same. Because the purpose of analysis was mainly to determine the maximum load and load-deflection behavior up to the maximum load, the model was sufficient and met the objective of the study reasonably well. The correctness of the FE

model was checked by comparing the analysis results with the test data. Once the correct material properties and element size were obtained, the models were expanded to study the behavior and strength of composite slabs with different slenderness.

The ABAQUS/Explicit solver was chosen for the analysis because it has a BRITTLE CRACKING model which is most suitable for modeling the tensile cracking of plain concrete in composite slabs. According to Abaqus (2002), the brittle cracking model is designed for applications in which the behavior is dominated by tensile cracking. It assumes that the compressive behavior is always linear elastic and this assumption is most accurate in applications where the brittle behavior dominates. The model also allows automatic removal of zero stress elements after cracking so that excessive distortion of that element and subsequent premature termination of the simulation can be avoided.

5.4.1 Structural model

Slab 3VL16-8-7.5 from the small scale tests was chosen for the preliminary development of the FE model. A one foot wide strip of the slab is shown in Fig. 5.1(a) and the cross section is shown in Fig. 5.1(b). Because of the symmetric condition, only one-quarter of the strip, as shown in Fig. 5.1(c), was considered in the FE model.

The concrete slab was modeled with 8-node linear brick, reduced integration elements (C3D8R) while the steel deck was modeled with 4-node doubly curved shell, reduced integration finite membrane strains elements (S4R). The steel deck elements located underneath the concrete slab elements were offset from the bottom of concrete elements at a distance half of the steel sheeting thickness. Fig. 5.2 depicts the slab model with the steel sheeting offset away from the concrete element for clarity.

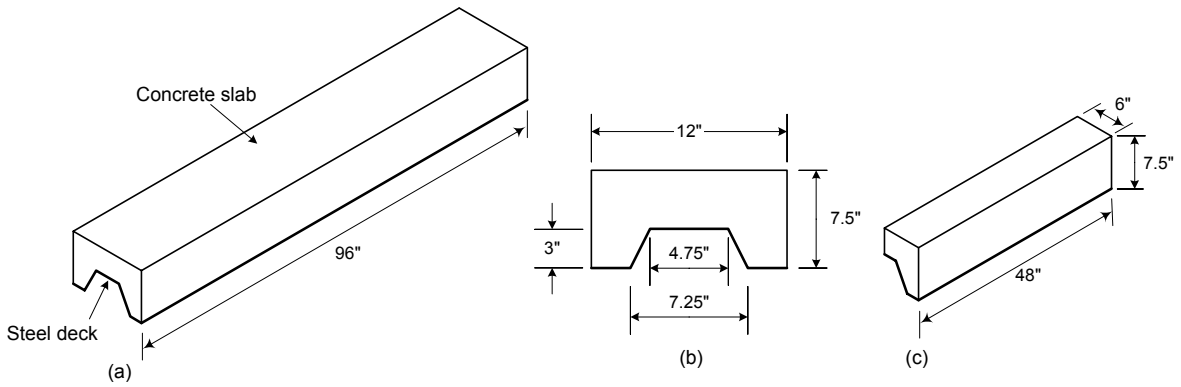

Fig. 5.1 Composite slab for 3VL16-8-7.5
(a) One-foot strip, (b) Cross section, (c) One-quarter model.

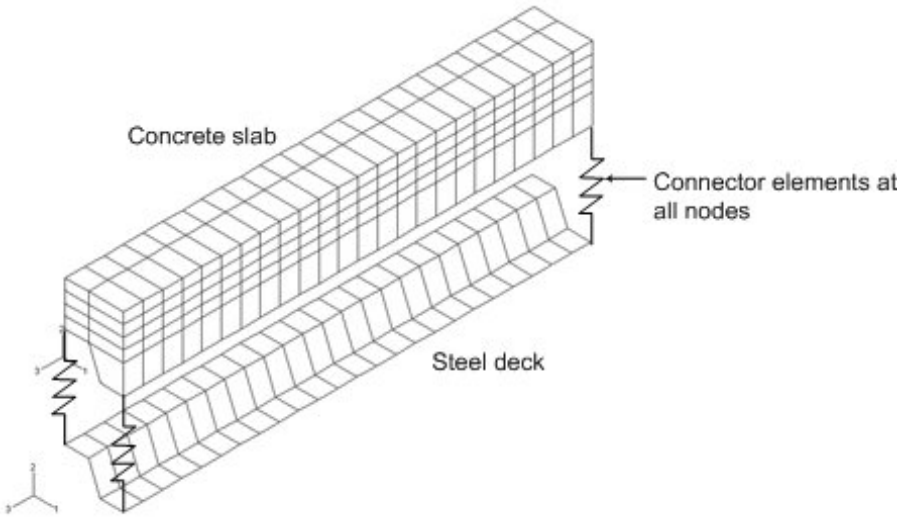

Fig. 5.2 FE model

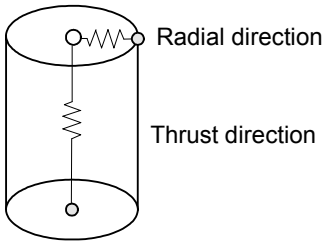

Fig. 5.3 Radial-thrust connector element

The interaction between the concrete and steel deck was modeled with radial-thrust type connector elements (CONN3D2). A connector element connected the concrete and steel nodes that were closest to each other. The use of radial-thrust elements enabled the behavior for radial and thrust displacements to be specified separately as shown in Fig. 5.3. The radial component was orientated in the longitudinal direction of the slab while the thrust component was for the vertical interaction. The horizontal shear interaction property, derived from the small scale tests, was assigned uniformly to the radial thrust components. The vertical interaction was not considered in the model assuming that its effect was implicitly present in the horizontal shear property. This assumption was made because the horizontal shear property was derived directly from the bending test. For the same reason, the frictional resistance at the support was also excluded in the model. A relatively stiff value was assigned to the thrust component of the connector elements so that the concrete and steel elements would not overlap when the load was applied.

A roller support was provided at 4 in. from the slab end and was applied to the nodes of the bottom flange of steel sheeting. Nodes at the side faces of the concrete, at the edges of the steel sheeting along the slab length, and at the mid-span were given appropriate boundary conditions to simulate the continuity of the slab in the lateral direction and the half span model in the longitudinal direction.

5.4.2 Concrete properties

All concrete elements except those in the top layer were modeled with the BRITTLE CRACKING function. This model considered the concrete behavior to be predominantly governed by tensile cracking. As mention earlier, the model also assumed that the compressive behavior was always linear elastic. This assumption was consistent

with the observation of slab behavior during the test (see Sec. 3.3 and conclusion 3 of Chapter 3) where the concrete did not fail by crushing but rather separated by excessive tensile cracking due to slip. The same observation was reported by Luttrell (1987). The concrete elements in the top most layer were assigned a linear elastic property where no cracking was allowed. This was done to avoid convergence problems where the model could become numerically unstable before reaching ultimate load if the crack was allowed all the way up to the top most layer.

The basic concrete properties and brittle cracking parameters were assumed based on various literature and the final values were fixed after an admissible result was obtained. The final concrete properties are given in Table 5.1.

Table 5.1 Concrete mechanical and brittle cracking properties used in the FE model.

Concrete Properties	Values
Density	0.000255 $lbfs^2/in^4$ (2400 kg/m^3)
Elasticity modulus	$3.60x10^6$ psi (24.8 GPa)
Poisson ratio	0.2
Cracking failure stress	300 psi (2.07 MPa)
Mode I fracture energy	0.42 lb/in. (73.56 N/m)
Direct cracking failure displacement	0.0005 in. ($1.27x10^{-5}$ m)
2 segments tension stiffening model	Remaining direct stress, Direct cracking displacement. 300.0 psi, 0.0 in. 90.0 psi, 0.00088 in. 0.0 psi, 0.0055 in.
Post cracking shear behavior model	Power law with 2.0 power factor 0.4 % maximum crack opening strain for coarse mesh. The value was adjusted proportionately according to characteristic mesh size for models with different mesh sizes.

5.4.3 Steel sheeting properties

Veljkovic (1994) reported that the indentations pressed in the web reduced the effective yield stress and the elastic modulus to 47% of the original values of the flat sheet. Strain gage readings from full scale tests, as presented in Sec. 3.10, confirmed that at some point during the load application the bottom flange of the steel deck yielded. In this study, both linear elastic and elastic-perfectly plastic behavior that uses Von Mises yield surface were tried. Several reduced yield stress and modulus of elasticity values for the web elements were tried. An elastic-perfectly plastic model with web yield stress and modulus of elasticity reduced by 50% of the flange values produced results that correlated well with test data. The final properties of the steel sheeting are given in Table 5.2.

Table 5.2 Steel properties used in the FE model

Steel properties	Values
Density	0.0007299 $lbfs^2/in^4$ (7800 kg/m^3)
Elastic modulus (flanges)	$29.5x10^6$ psi (203.4 GPa)
Yield stress (flanges)	50000 psi (345 MPa)
Elastic modulus (web)	$14.75x10^6$ psi (101.7 GPa)
Yield stress (web)	25000 psi (173 MPa)

5.4.4 Horizontal shear interaction property

The interaction property between the concrete and steel deck in the form of horizontal shear stress versus end slip was obtained from small scale test series #2 (see Sec. 2.7.3). The calculations were carried out in accordance with the work and force equilibrium methods as discussed in Sec. 4.6.1 and 4.6.2. A typical property is shown in Fig. 5.4. The

average relation from test A and B was used and converted into force versus slip for assignment into the connector elements. The interaction forces obtained from both work and force equilibrium methods were applied for analysis and the property that gave better calibration with the test results was chosen for implementation in further analysis.

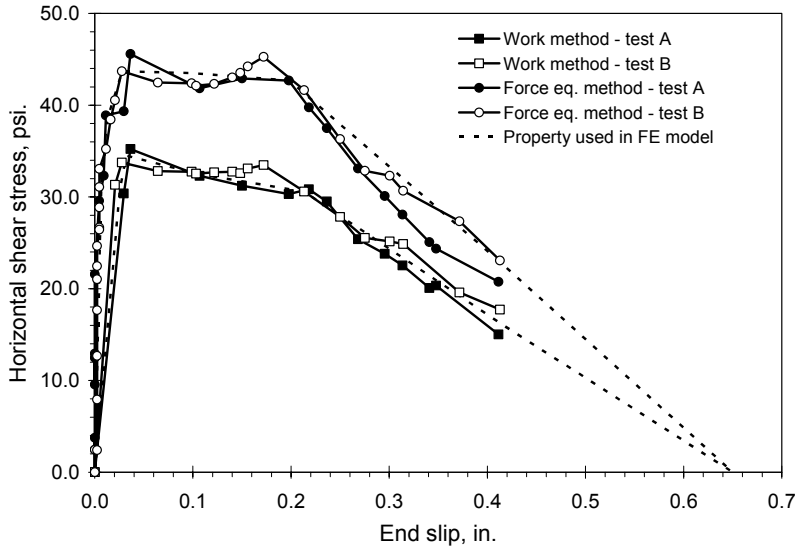

Fig. 5.4 Horizontal shear stress versus end slip for 3VL16-8-7.5s

5.4.5 Loading and solution control

Because ABAQUS/Explicit is a dynamic analysis program, and in this case a quasi-static solution is desired, the slab was loaded slowly enough to eliminate any significant inertia effect. The load was applied by specifying a displacement value at concrete top fiber nodes where the actual line load was acting. The displacement was increased linearly using a smooth amplitude function over a time step period of five to ten times longer than the natural period of the structure. This was done to ensure that the quasi-static results were obtained. The natural period was obtained by performing eigenvalue frequency analysis which is available in ABAQUS/Standard module. Longer loading periods can reduce

dynamic effects but may increase analysis time significantly. An optimum analysis period was obtained after several trials.

Before any result was accepted, the kinetic energy was compared with internal energy of the whole model throughout the analysis period to give a general indication whether quasi-static solution was obtained. The quasi-static response was ensured by keeping the kinetic energy below 5% of the internal energy at any instance during analysis and this was done by adjusting the loading period and total displacement at loading nodes accordingly. A sample of an ABAQUS input file is given in Appendix E.

5.5 Analysis results and interpretation

Analyses using the coarse mesh shown in Fig. 5.5 on 3VL16-8-7.5s specimen were carried out to determine good combinations of material properties and to obtain admissible quasi-static solutions. The shear interaction property was first taken from the force equilibrium method as shown in Fig. 5.4. For each combination of material properties, the analyses were performed by varying the time step period and total deflection at loading nodes.

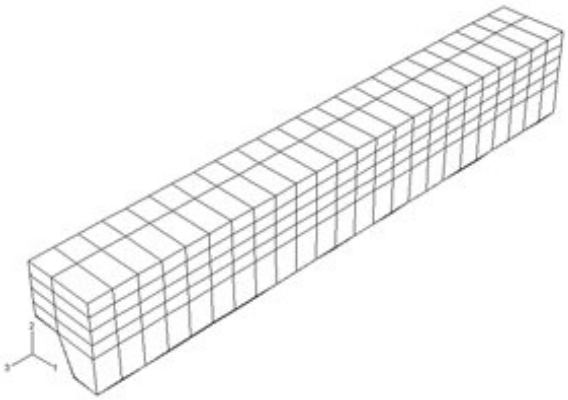

Fig. 5.5 Coarse mesh for 3VL16-8-7.5

For each result, internal and kinetic energies of the whole model were plotted. Fig. 5.6(a) depicts the typical internal and kinetic energy levels during the analysis period for the dynamic response while Fig. 5.6(b) is for the quasi-static response. The corresponding reaction force versus mid-span deflection curves are shown in Fig. 5.7(a) and Fig. 5.7(b) respectively.

As mentioned before, the quasi-static response was assured by keeping the kinetic energy level below 5% of the internal energy level. However, because ABAQUS/Explicit is a dynamic analysis program, oscillating response was inevitable even in the quasi-static solution. The oscillation magnitudes became larger for smaller step time period but reduced as the step time period increased. The quasi-static results were generally obtained when the time step periods were longer by 5 times or more than the slab natural period. The results were then smoothed using the smoothing function available in ABAQUS CAE as shown in Fig. 5.7(b) to eliminate the oscillation effect.

Three element sizes designated as coarse, medium and fine, as shown in Fig. 5.8 were tried for 3VL16-8-7.5 in the early development of the model using the same material properties listed in Table 5.1 and 5.2 to illustrate mesh sensitivity. The connector elements for the fine mesh were located at the same locations as for the coarse and medium mesh models, that is at 2 in. interval along the longitudinal length. Results of the analyses together with test data are shown in Fig. 5.9. The graphs show that the models were insensitive to the element size. However the coarser mesh model responded more sensitively to the change of time step period as reflected by a greater vibration magnitude than the finer mesh model.

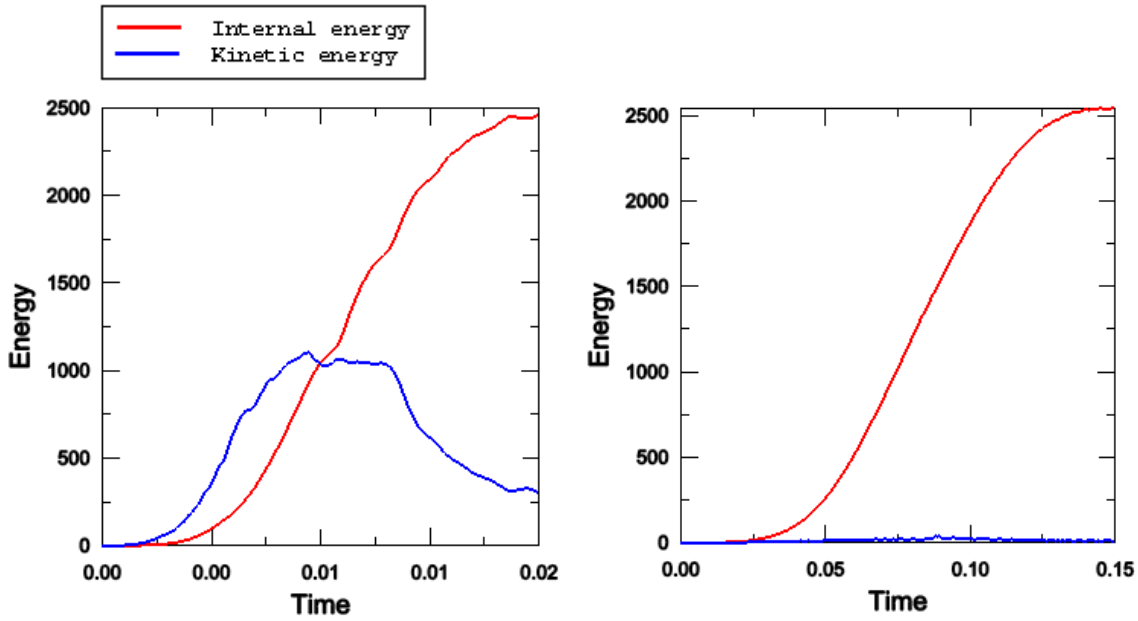

Fig. 5.6 Energy level for analysis with step time equal to (a) 1x natural period (b) 8x natural period

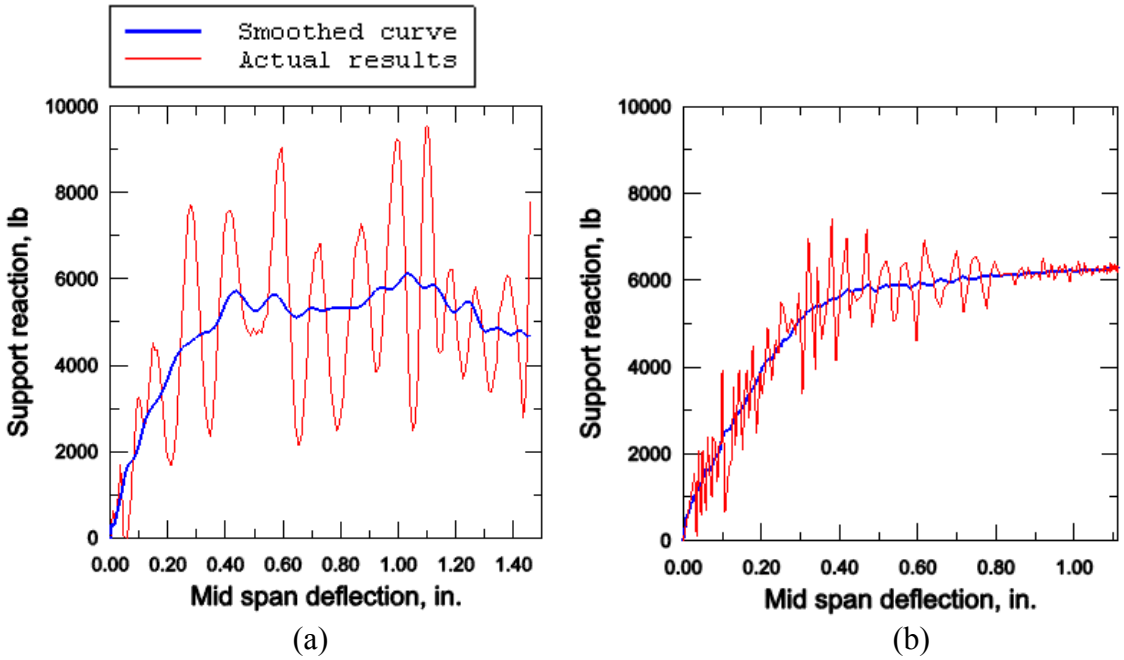

Fig. 5.7 Typical analysis results (a) Dynamic response, (b) Quasi-static response

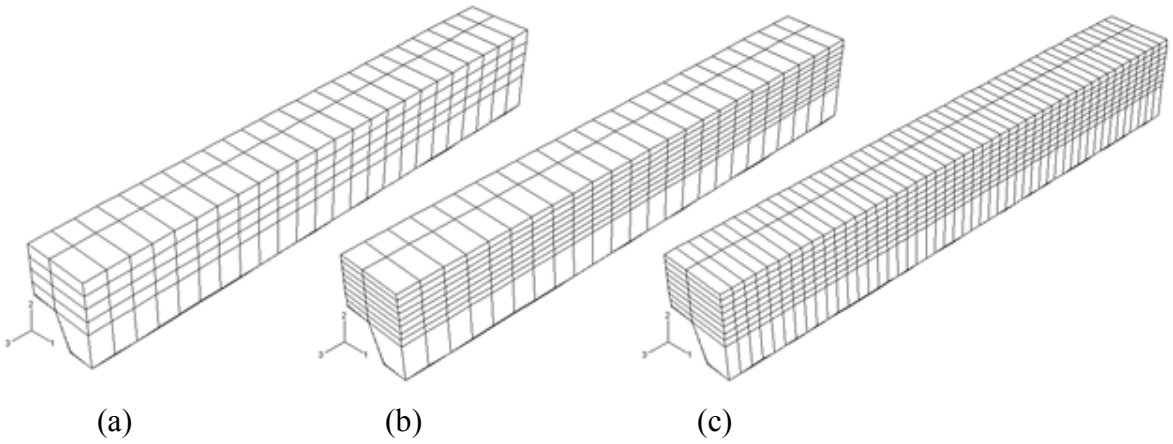

(a) (b) (c)

Fig. 5.8 FE model for 3VL16-8-7.5 slab
(a) Coarse, (b) Medium and (c) Fine elements

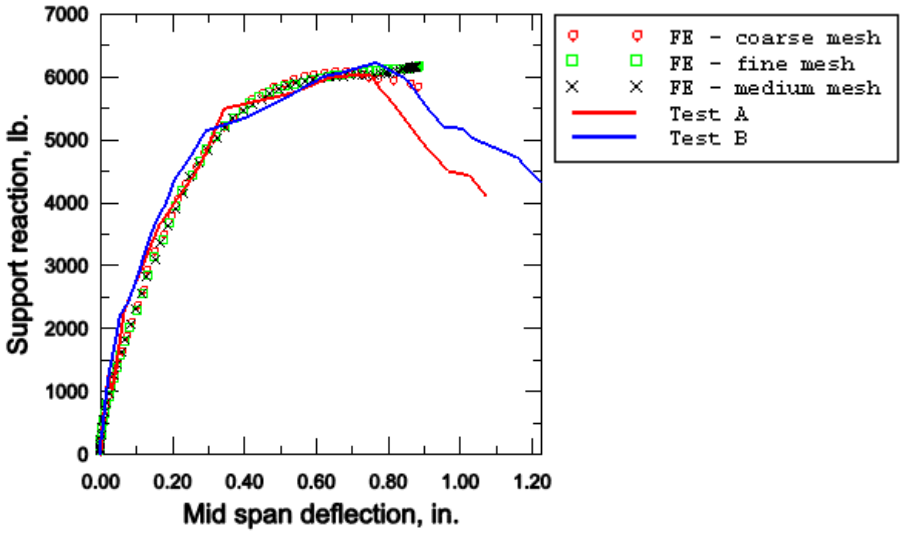

Fig. 5.9 Results of analyses using coarse, medium and fine meshes.

Fig. 5.10 shows the results of analysis of the same slab using a fine mesh model but using the interaction property calculated by work method. It shows clearly that the interaction property obtained by work method was too conservative compared to the test data. Based on this observation, only the property obtained by the force equilibrium method was used in subsequent analysis.

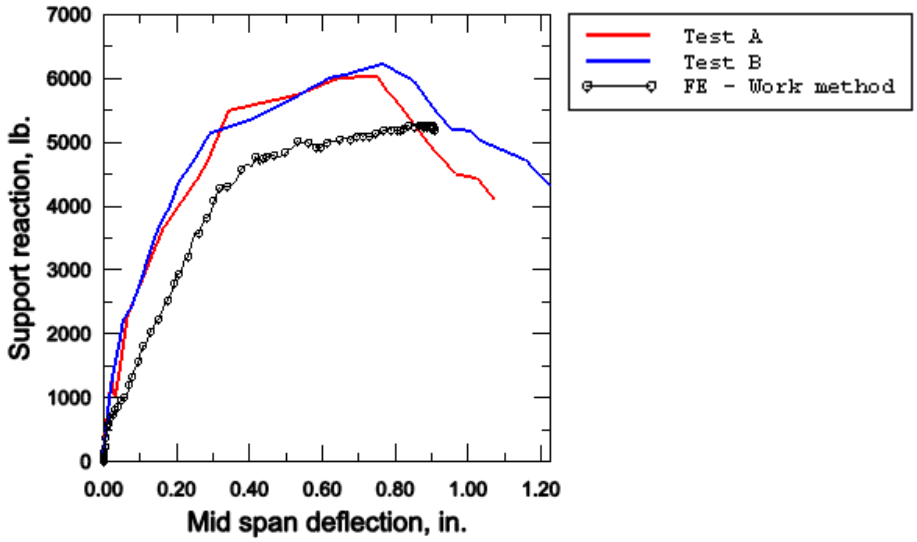

Fig. 5.10 Results of analysis with interaction property calculated by work method

5.6 Verification of the FE model

To further illustrate the admissibility of the FE model, analyses were carried out on models 3VL16-4-7.5, 3VL16-10-7.5, 3VL16-12-5 and 3VL16-14-5 using the same material properties as before. The shear interaction properties for each model slab were calculated from the corresponding test data using the force equilibrium method. The horizontal shear stresses versus slips for each slab are shown in Fig. 5.11. The shape of the curves closely resembles the curve in Fig. 5.12, which was from push off test data reported by Veljkovic (1993). Analysis results are plotted together with the test data as in Fig. 5.13(a) to (d). The graphs indicate that the FE models predict the behavior of each slab with acceptable accuracy.

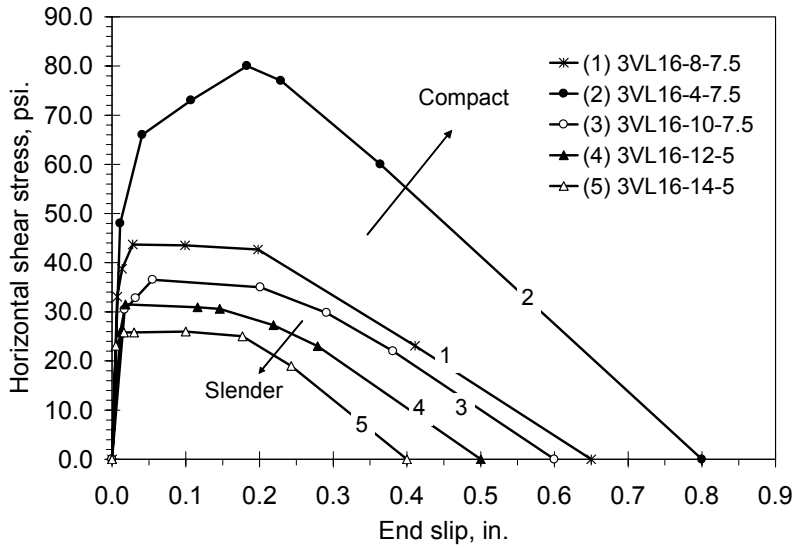

Fig. 5.11 Horizontal shear stress versus slip for 3VL16 slabs calculated from small scale test data using force equilibrium method.

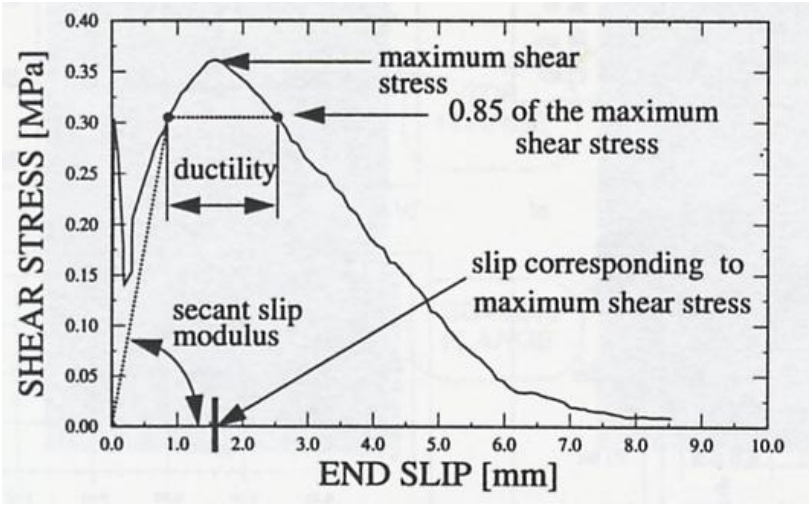

Fig. 5.12 Shear stress versus slip (after Veljkovic, 1993)

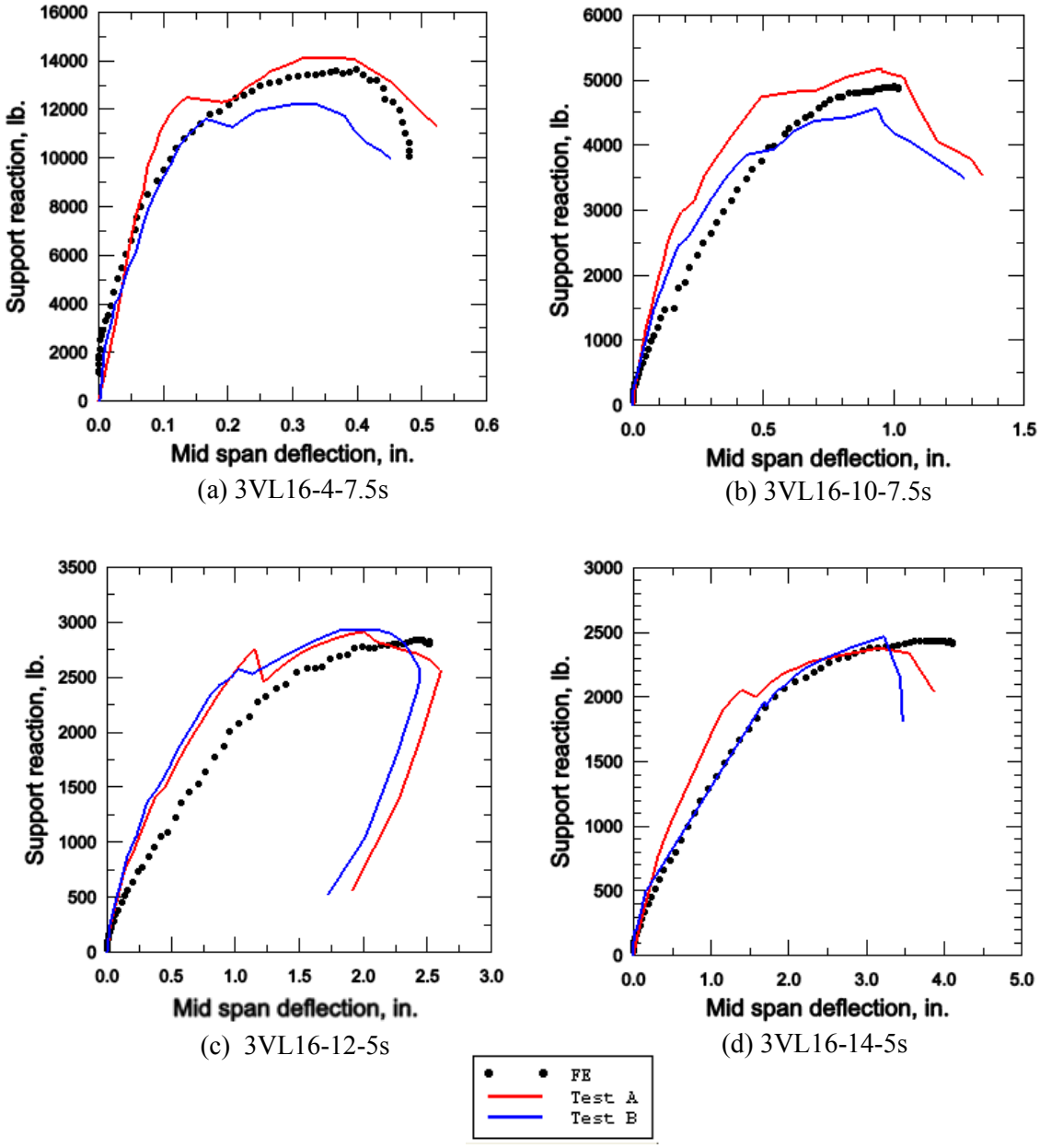

Fig. 5.13 FE and test results of slabs 3VL16

5.7 Critical issue regarding horizontal shear force-slip relationship

As depicted in Fig. 5.11 the shear bond property varies with slab configuration, in which the amount of stress and slip are larger for compact slabs and the quantities become smaller when the slab slenderness increases. The property is therefore unique to a particular slab dimension and is not interchangeable to other slab dimensions. The FE results reported in the previous section indicated that accurate results for a particular slab can only be obtained when the shear bond-slip property from the same slab is used.

To further illustrate this finding, analyses were performed again on models 3VL16-4-7.5, 3VL16-10-7.5, 3VL16-12-5 and 3VL16-14-5 using only one shear bond-slip property (from slab 3VL16-8-7.5) which is represented by graph #1 of Fig. 5.11. The results are added to those shown in Fig. 5.13 and are presented in Fig. 5.14. It is clear from the results that the use of shear bond-slip obtained from slab 3VL16-8-7.5 underestimated the capacity of the more compact slab, namely 3VL16-4-75, but overestimate the slenderer slabs, namely 3VL16-10-7.5, 3VL16-12-5 and 3VL16-14-5.

It is evident from the results presented above and in the previous section that with a right combination of material properties, the use of a single shear bond-slip relationship may produce good results for one particular slab geometry only but it may not be so accurate when the slab slenderness and geometry are changed. All FE and other rigorous analysis of composite slabs performed by many researchers in the past used a single shear bond-slip property obtained from conceptually the same push off type tests. Tenhovuori and Leskela (1997, 1998) even conducted the FE analysis using an assumed non-variable shear bond-slip relationship on various slab geometries. While those analyses showed some

degree of success, almost all reports did not provide sufficient information regarding the accuracy of the analysis with respect to variable geometry models.

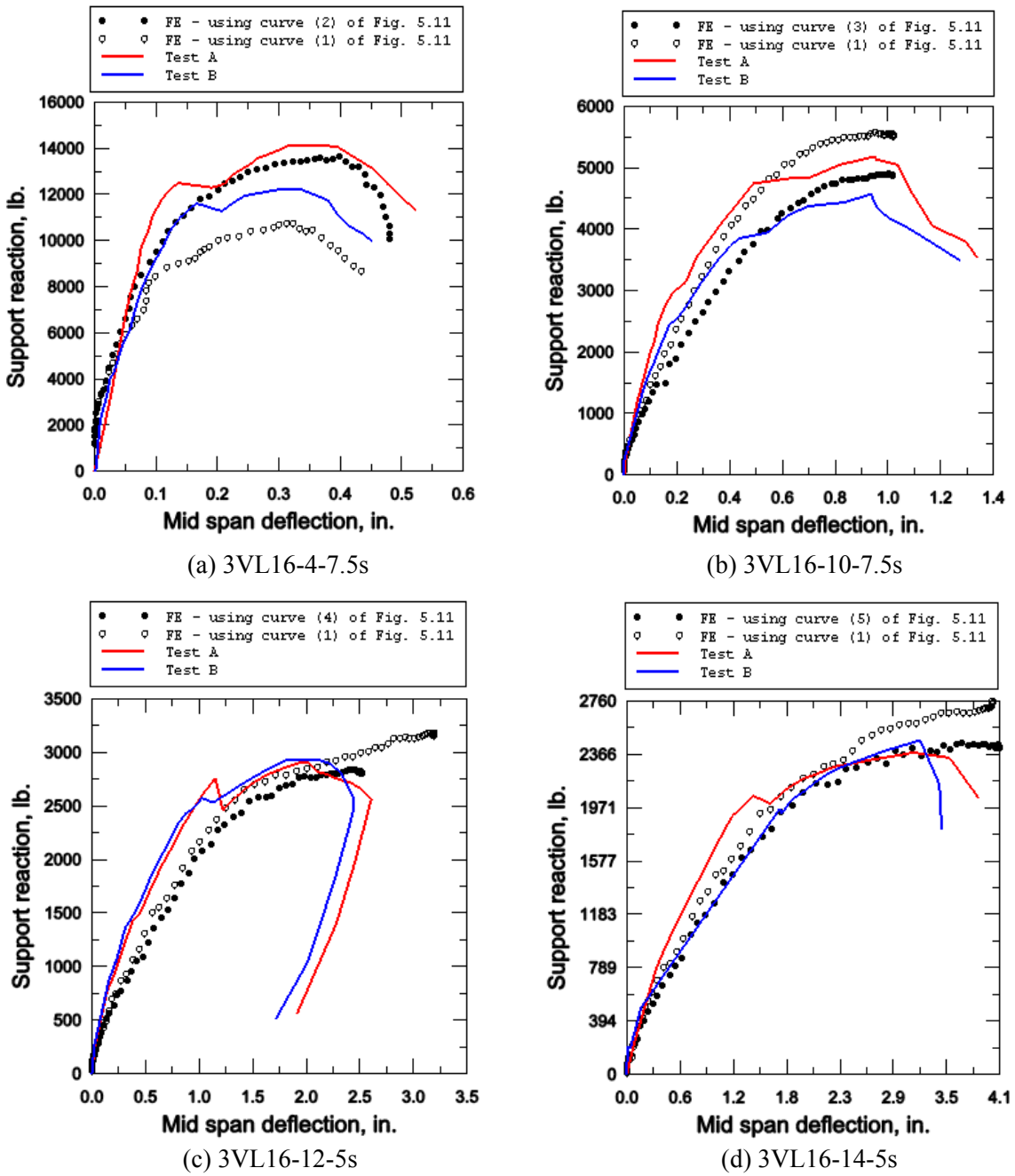

(a) 3VL16-4-7.5s

(b) 3VL16-10-7.5s

(c) 3VL16-12-5s

(d) 3VL16-14-5s

Fig. 5.14 Comparison of analysis results for slabs in Fig. 5.13 using individual shear bond-slip and shear bond-slip curve #1 of Fig. 5.11.

An (1993), who used the shear property obtained from block bending test for analysis of slabs of different slenderness, found that the FE results were good for long span slabs. However she also stated in her conclusion that "The numerical analysis underestimated the capacity of the slabs which were tested with the short shear span". She stated that the inaccuracy of the short slab results was due to the friction force at the support not being included in the model. However if the friction force was included in the long span model, her results could have been well overestimated and incorrect as well.

As discussed in Sec 5.3, Veljkovic (1995) had to do three types of small scale tests to obtain a good model for the shear interface property (see also Sec. 2.3.9). To achieve a correct simulation, a function was used to reduce the interfacial shear stress level during the analysis depending upon the strain level in steel sheeting. This modification is clear evidence regarding the need for variable shear interface properties when dealing with variable geometry models. If an automatic reduction function was not included in the FE package, the FE analysis conducted this way requires user intervention to modify the interface property several times along the analysis process. With so many tests to be conducted, the process of conducting FE analysis in this manner would require significant additional effort.

Shortcomings of FE modeling as discussed above can be attributed to the use of single shear interaction property obtained from push off type tests. These tests do not represent the true behavior of slab bending where clamping, slenderness and curvature are not present. Additionally, push tests may also over estimate the shear force because the deck is usually fixed to the support and restrained from moving. This is not representative of actual slab behavior. The inaccuracy can magnify when the concrete is restrained from

separating from the steel deck by the application of lateral load (Stark, 1978; Daniels, 1988). Friction forces at the supports must also be included in the FE model because this property is not accounted for in the push test. This requires the use of additional tests such as the slip block type (Patrick and Poh, 1990).

5.8 Concluding remarks

1) The brittle cracking model in ABAQUS/Explicit is sufficient for modeling concrete tensile cracking in composite slab.

2) The small scale test procedure developed in this research is reliable and applicable with the present design methods. It has the potential for replacing the full scale performance test as well as to become a more accurate tool for determining the shear bond property used in numerical analysis.

3) FE Modeling of composite slabs has become easier and more accurate using data from the small scale bending test because parameters that influence the slab behavior such as steel deck strain, support friction, slenderness, and curvature have already been included implicitly in the shear bond property.

4) The force equilibrium method proposed in Chapter 4 is an admissible tool for calculating the shear bond property in slabs under bending.

5) The shear bond property is unique to slab geometry and the value must be adjusted according to slab geometry to obtain correct numerical analysis.

6 Modeling of the horizontal shear bond stress

6.1 Introduction

It has been shown in the previous chapter that the shear bond property of composite slabs is geometry dependent and the correct property must be used to model a particular slab in the numerical analysis, so that an accurate prediction of the slab strength and its behavior can be obtained. If this is the case, then modeling composite slabs by the FE method would become uneconomical because tests would need to be conducted for every slab before they can be correctly modeled. Therefore it is essential to establish a method for estimating the shear bond property that is applicable to variable geometry slabs without a need for too many tests.

6.2 Objective

The first objective of this chapter was to devise a method for estimating the shear bond property for slabs of any dimension based on the smallest number of tests. In doing so, data from the small scale bending tests as presented in Chapter 4 will be used throughout this study. After devising the method, the estimated property will be applied in the FE models and the analysis results are verified by comparing them with the test data. The next purpose of this study is to examine more closely the mechanism of shear bond stress and its relation with the slenderness of the slab and how this mechanism affects the

accuracy of the present PSC methods. From the results of this study, an improvement to the PSC method will be suggested.

6.3 Method for estimating the shear bond stress-slip property

6.3.1 Establishing a relationship between shear bond stress and slenderness

For slabs exhibiting a shear-bond failure mode, the ultimate shear bond equation is given by ASCE (1992) in the form of the *m-k* equation:

$$\frac{V}{bd\sqrt{f'_c}} = m\frac{\rho d}{L_s\sqrt{f'_c}} + k \tag{6.1}$$

By removing the concrete compressive strength and substituting the reinforcement ratio with $\rho = \frac{A_s}{bd}$, Eq. 6.1 becomes;

$$\frac{V}{bd} = m\frac{A_s}{bL_s} + k \tag{6.2}$$

Equation 6.2 is the version of the *m-k* method used in Eurocode 4 (1994). It has been shown in Chapter 3 that Eq. 6.2 produces less dispersion in the results than Eq 6.1. This is in agreement with the findings of previous research in which the reason is attributed to the concrete strength (Johnson, 1994). It was found that Eq. 6.1 can give unsatisfactory results for the *m* and *k* values if the concrete compressive strength varies widely within a series of tests. According to Seleim and Schuster (1985), neither the reinforcement ratio nor the concrete compressive strength had a significant influence on the shear bond resistance, but the steel thickness was a governing parameter. Work reported by Luttrell (1987), Daniels (1988), Bode and Saurborn (1992) and Veljkovic (1995) also confirmed that the concrete strength did not influence the slab behavior and strength significantly. The

removal of f'_c from Eq. 6.1 and the use of Eurocode's equation for designing composite slab is therefore justified.

Consider the free body diagram in Fig. 6.1 for the typical shear bond failure as assumed in the partial shear connection theory. By taking moments about the compressive force, *C* and considering that the moment arm differs very slightly from the slab effective depth, the moment equilibrium equation can be estimated as;

$$VL_s = Td + M_r \tag{6.3}$$

Substituting *T* with $\tau(L_s+L_o)b$, Eq. 6.3 becomes;

$$VL_s = \tau(L_s + L_o)bd + M_r \tag{6.4}$$

where,

V = reaction or vertical shear force

L_s = shear span length

L_o = overhanging length

τ = shear bond stress

b = slab width

d = effective depth

M_r = remaining moment strength in the deck.

Equation 6.4 is approximate because the lever arm is always less than the effective depth. Nevertheless, for composite slabs the difference is insignificant because after shear slip has taken place, the crack tip grows upward bringing the composite neutral axis close to the top fiber.

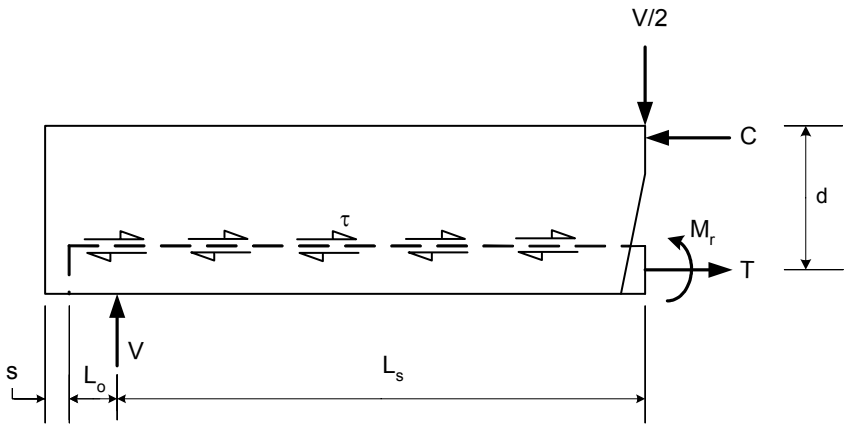

Fig. 6.1 Free body diagram for slab along the shear span which fails by shear bond

Rearranging Eq. 6.4 into $V = \frac{\tau(L_s + L_o)bd + M_r}{L_s}$ and substituting it into Eq. 6.2 a new equation relating shear bond stress to the slab geometry is obtained;

$$\tau d = m\frac{A_s}{b}\frac{d}{\left(L_s + L_o\right)} + \left(\frac{kbdL_s - M_r}{b\left(L_s + L_o\right)}\right) \tag{6.5}$$

In the FE study the width, *b* considered in the above equation is the actual cross section length of the steel deck per one unit width of small scale specimen (see Fig. 6.2). Therefore, for a unit width model, $\frac{A_s}{b}$ is equal to the thickness, *t* of the steel deck;

$$\tau d = m\frac{td}{\left(L_s + L_o\right)} + \left(\frac{kbdL_s - M_r}{b\left(L_s + L_o\right)}\right) \tag{6.6}$$

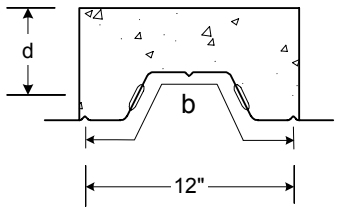

Fig. 6.2 Slab cross section considered in the FE model

It should be noted that the derivation of Eq. 6.6 is based on the uniform distribution of shear stress, τ, over the actual surface area of the steel deck and along the length measured from the applied load to the slab end.

When deriving the original *m-k* equation, Schuster 1970 neglected the contribution of the remaining moment strength, M_r in the steel deck and so did Patrick (1994), Veljkovic (1996b) and Widjaja and Easterling (1996) for their modified PSC methods. For deck profiles with re-entrant shape, which is popular in Europe and Australia and used to a limited degree in the United States, the contribution of M_r is negligible, because the deck depth is usually small and the moment capacity of such profiles is low. This is evident by looking at the required shoring to support the concrete and construction load during construction. For trapezoidal profiles which are popular in the United States, the United Kingdom and other parts of the Europe, the contribution of M_r can be significant, especially near the ultimate load. The behavior beyond ultimate load is also influenced by M_r. It will be shown in this part of the study that the last term in Eq. 6.6 is constant regardless of the value of M_r and therefore a determination of the term here is not needed. Equation 6.6 can be simplified to;

$$\tau d = m\frac{td}{\left(L_s + L_o\right)} + k \tag{6.7}$$

The overhanging length, L_o is usually short. It is assumed here that L_o is not a determining factor for the slab behavior and therefore it can be removed from the equation. However its contribution to the horizontal shear resistance cannot be neglected and it should be included when τ is calculated either using the PSC method (refer Eq. 4.11) or using the force equilibrium method as discussed earlier.

Therefore Eq. 6.7 becomes;

$$\tau d = m\frac{td}{L_s} + k \tag{6.8}$$

Equation 6.8 is linear, similar to the *m-k* design equation with τd on the vertical axis and $\frac{td}{L_s}$ on the horizontal axis. To facilitate extensive reference to Eq. 6.8 in the rest of this report, and to differentiate variable *m* and *k* from the *m-k* method, Eq. 6.8 is subsequently referred to as the *shear bond-slenderness* equation and the slope and the intercept are changed to *p* and *s*. The choosing of *p* and *s* is made to carry the connotation of partial shear connection because the equation just derived will be used later in the PSC method. The term $\frac{d}{L_s}$ is defined as *slab compactness* while its inverse, $\frac{L_s}{d}$ is already known as *slab slenderness*. The shear bond-slenderness equation now becomes;

$$\tau d = p\frac{td}{L_s} + s \tag{6.9}$$

6.3.2 Verification of the shear bond-slenderness equation with the test data.

Maximum shear stresses were calculated for all specimens 3VL and 2VL from small scale tests (Table 4.4) using the force equilibrium method. The results are plotted on the shear bond-slenderness axis as shown in Fig. 6.3 and Fig. 6.4 respectively. All results fall along the straight lines which confirm the accuracy of the equation. Using the regression line, one can find the *p* and *s* values to calculate the maximum shear bond strength of slabs built on similar profile but of different thickness, length and depth.

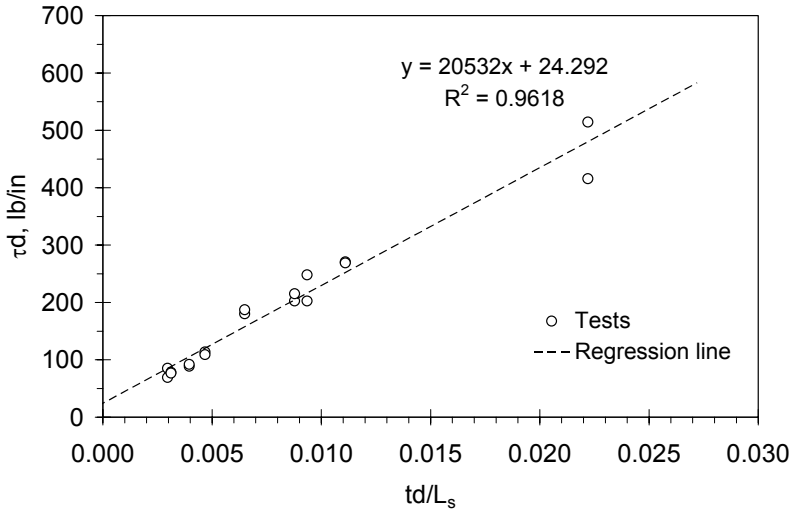

Fig. 6.3 Plot of τd versus td/L_s for small scale specimens built on 3VL decks

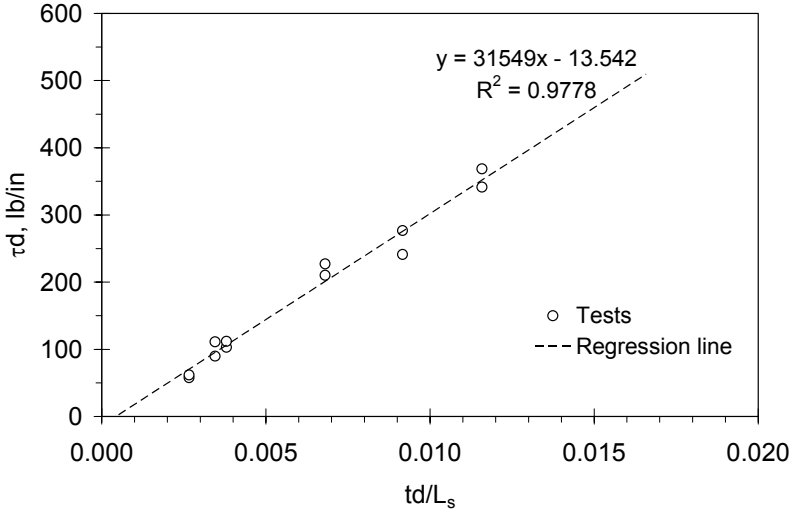

Fig. 6.4 Plot of τd versus td/L_s for small scale specimens built on 2VL decks

6.3.3 Interpolation method

It has been shown that the maximum shear bond stress for slabs of any slenderness built on the same deck profile vary linearly with the slab compactness. Based on this information, other points below the maximum value on the shear bond stress-slip curve are also assumed to be linear. As such they can be estimated by linear interpolation between two known curves derived from the tests. The interpolation follows the same proportion as for the maximum shear stresses.

To illustrate the interpolation procedure, consider the shear bond stress-slip curves from specimen 3VL16-4-7.5 and 3VL16-14-5 of Fig. 5.11. The shear bond stress-slip relationship for slab 3VL16-10-7.5 is to be determined by interpolation using these two curves. The interpolation method is depicted graphically in Fig. 6.5. The maximum shear stress, τ_3, that lies on curve 3VL16-10-7.5 is first obtained from regression line of Fig. 6.3. After knowing τ_3 the corresponding slip, s_3 can be determined easily by linear interpolation between maximum points of curves 3VL16-4-7.5 and 3VL16-14-5 whose coordinates are (s_1, τ_1) and (s_2, τ_2) respectively. The next nearest point on curve 3VL16-10-7.5 is assumed to lie along the straight line between the next nearest points on curves 3VL16-4-7.5 and 3VL16-14-5. The position of this point is at an equal proportion as for the maximum stress points calculated before, such that $\frac{a}{b} = \frac{c}{d}$. By linear interpolation the coordinate of the new point can be calculated. Likewise, other points on curve 3VL16-10-7.5 can be determined in a similar manner. For comparison, the shear stress-slip curve for 3VL16-10-7.5 obtained from tests data also drawn in Fig. 6.5. As depicted in the figure, both curves especially the values near the maximum region are in good agreement. The difference between the

interpolated and the calculated curves beyond maximum value will not influence the analysis results significantly because the FE model carried out in this study was only accurate up to the maximum load (see Sec. 5.4).

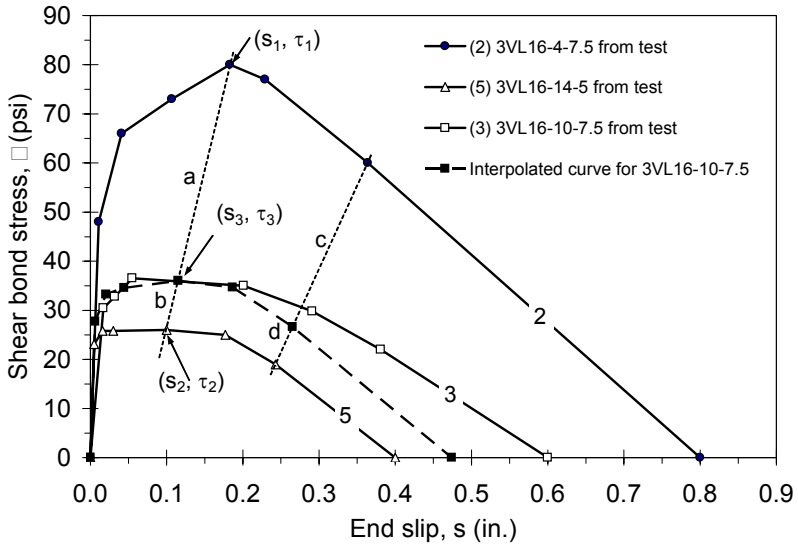

Fig. 6.5 Estimating shear stress-slip curve by linear interpolation

6.3.4 Application of the shear bond model in the FE element analysis

The shear bond stress-slip properties of slabs 3VL16-4-7.5 and 3VL16-14-5, which were derived from small scale tests (curve 2 and 5 of Fig. 6.5) were used to estimate the shear bond stress-slip property for a series of slabs 3VL16 by the interpolation method as discussed above. Some of slab geometries were similar to the tested specimens plus several other sizes which were chosen arbitrarily so their slenderness values would fill the gaps between the tested slenderness. The interpolated shear bond properties for these slabs are shown in Fig. 6.6. Note that in this figure, an additional number was added to the slab label to indicate the shear span length measured in inches. Finite element analyses were performed on these models utilizing the same material properties as given in Table 5.1 and

5.2. The analysis results in the form of maximum support reaction due to applied load versus the slenderness are plotted in Fig. 6.7. Test data are also plotted in the same figure for comparison. The curves fitted to both data series using power function are almost identical indicating that the FE models using interpolated shear bond property were accurate.

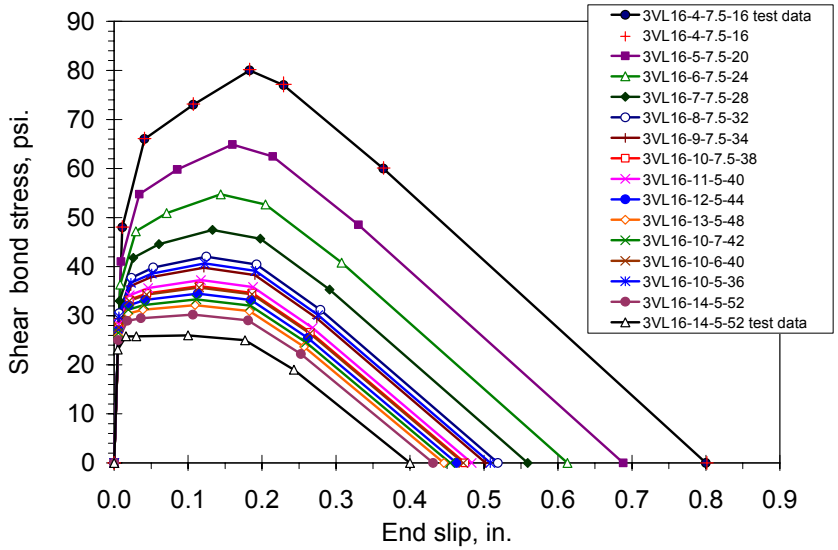

Fig. 6.6 Shear stress-slip property for 3VL16 slab of variable slenderness

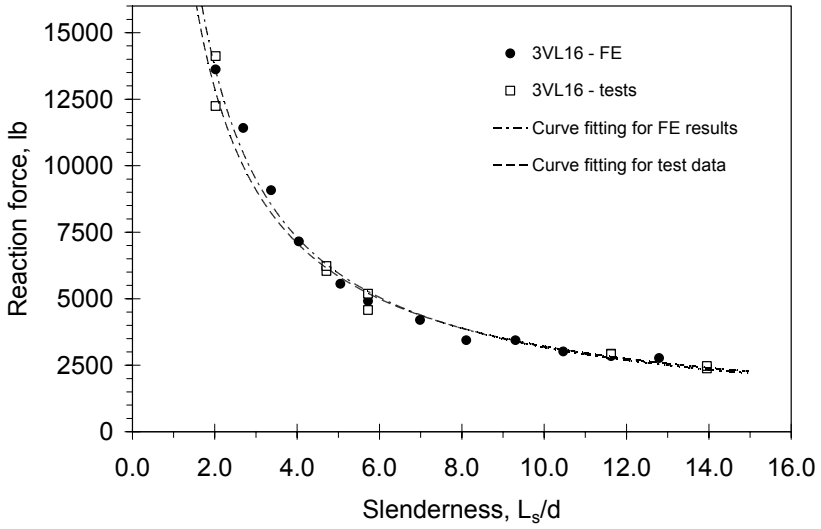

Fig. 6.7 Tests data and FE results for slab 3VL16 with variable slenderness

Two other slabs, namely 2VL20 and 3VL18 were analyzed in the same manner. Interpolation of the shear bond property for slab 2VL20 was based on small scale tests of specimen 2VL20-7-6.5 and 2VL20-9-4 while for slab 3VL18 the interpolation was based on specimen 3VL18-8-7.5 and 3VL18-13-5. In this exercise, the properties of slabs that were more compact and more slender than the tested specimens, for which the curve was based, could also be determined by extrapolation using the same procedure. The shear bond properties for model 2VL20 and 3VL18 are shown in Fig. 6.8 and Fig. 6.9 and the FE results are shown together with slab 3VL16 in Fig. 6.10. The results follow the same trend and compare well with each other.

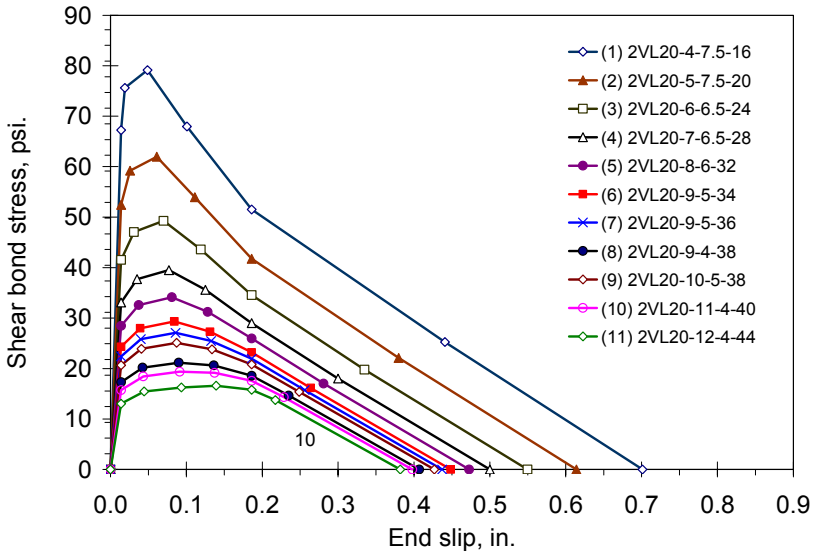

Fig. 6.8 Shear stress-slip property for 2VL20 slab of variable slenderness

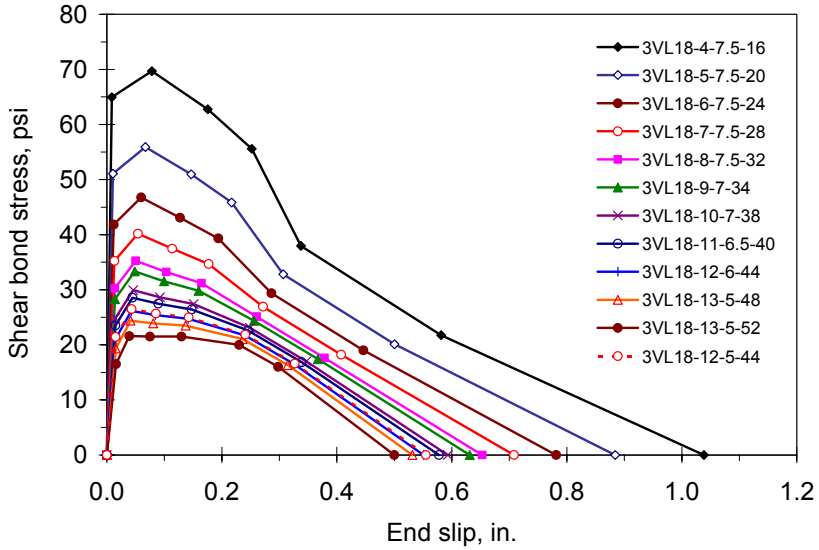

Fig. 6.9 Shear stress-slip property for 3VL18 slab of variable slenderness

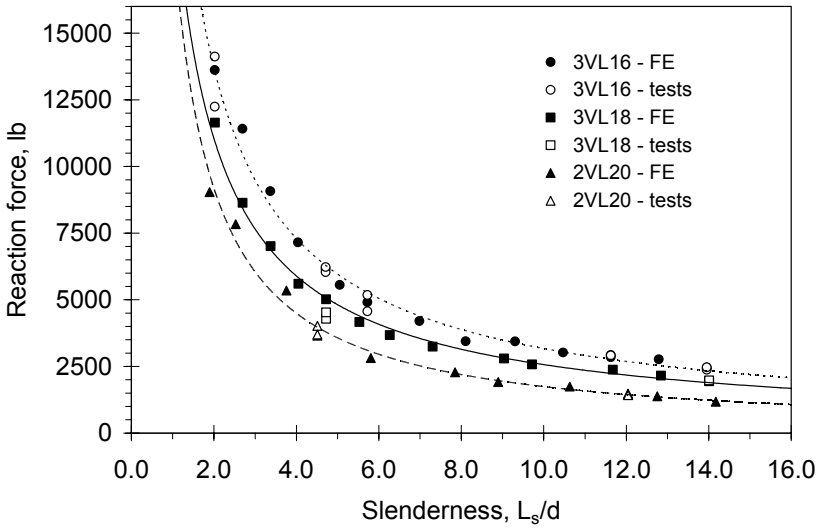

Fig. 6.10 Tests and FE results for slabs 3VL16, 3VL18 and 2VL20 with variable slenderness

6.4 Discussion on the shear bond stress characteristic

The derivation of the shear bond-slenderness equation opens up a new insight into understanding the mechanism of shear bond stress. It can be understood from the equation that for a given shear span, the shear bond strength is marginally affected by the change of effective depth. This is illustrated in Fig. 6.11, which depicts the plots of shear bond stress versus slip for slab 3VL16-10 with shear spans of 18, 24, 30, 36 and 40 in. For each value of shear span shown, the thicknesses were varied from 5 to 12 in. The values for shear bond stress were interpolated from the test data of specimen 3VL16-8-7.5-32 and 3VL16-14-5-52. The results indicate that the shear bond strength is reduced slightly by increasing the slab thickness. The change however did not alter the results of the FE analysis significantly. Hence, for a given shear span, an average value for the shear bond-slip relationship can be used for analysis of slabs of variable thickness.

Even though the shear bond strength does not change much with the effective depth, the slab load carrying capacity does. This is because the section properties and the moment arm are changed and not because of the varying shear bond. This behavior is similar to ordinary reinforced concrete beams where the beam effective depth does not influence the anchorage bond strength.

To illustrate this behavior, slabs 3VL16-10 with variable thicknesses whose shear bond-slip properties are shown in Fig. 6.11, were analyzed. For each shear span, the average shear bond property was used. The results in the form of reaction force versus effective depth were plotted in Fig. 6.12. It confirmed that the maximum load carrying capacity increased with the slab depth even though the shear interaction is constant.

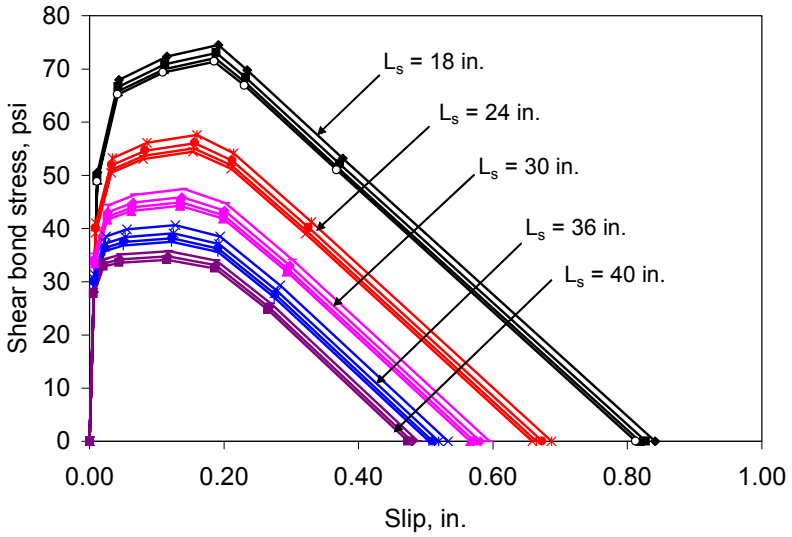

Fig. 6.11 Shear bond stress versus slip for slab 3VL16-10 with variable shear span and thickness

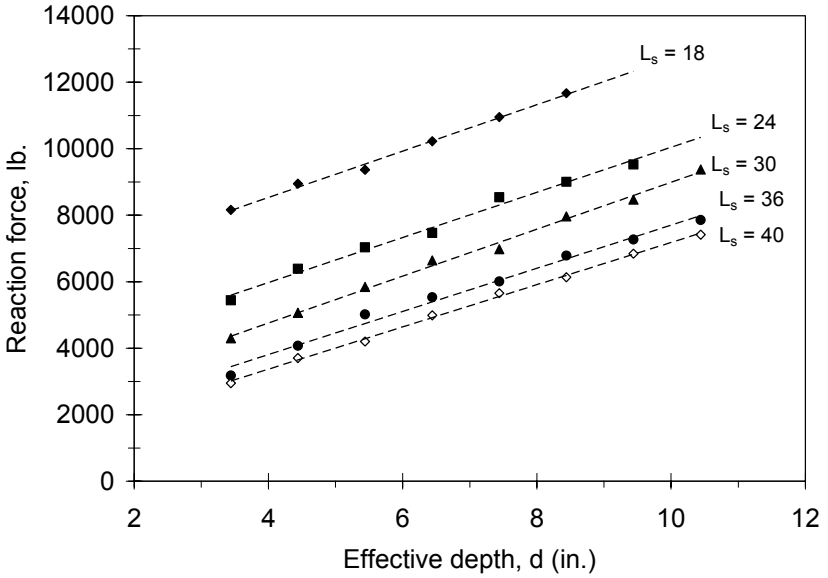

Fig. 6.12 Reaction force versus effective depth for slab 3VL16-10 with variable shear span and effective depth

It should be noted also that there is a limit for the slab thickness that can be considered in the variable thickness analysis as discussed above. Slabs that are too thick would not response linearly as in Fig. 6.12 because other effects such as direct load transfer to the support (refer Fig. 6.22) and deep beam effect may control the result of analysis.

The concept of invariable[5] shear bond strength with respect to depth alone is in disagreement with the popular belief such as that of Tenhovuori and Leskela (1998) who stated that the bond strength will increase when the effective depth is increased. They conducted a finite element study by assuming constant shear bond property in the steel-concrete interface and found that the shear bond kept increasing when the depth was increased. This can not be true because an increasing shear stress output contradicts the constant shear stress input. Looking at their results, it seems that the shear bond capacity can be limitless by increasing the slab thickness. In contrast, the shear bond capacity always has a maximum limit and the value depends on the slenderness of the slab as all test results have shown, especially for compact slabs where the failure mode is always horizontal shear slip. For slender slabs, which do not fail by shear bond, the reason is not because the shear bond strength is becoming higher but rather a larger interface area is available to mobilize enough shear resistance force so that the deck yields before the ultimate shear bond stress is achieved.

[5] Invariable shear bond strength referred to in this report means employing only one shear bond-slip curve for all slab models.

6.5 Improvement to the Partial Shear Connection (PSC) Method

6.5.1 Shortcoming of the PSC method

In the PSC method, the design parameter known as the degree of shear connection, η, is first determined through the partial interaction curve. The value η is read from the curve, as shown in Fig. 4.2(a), using the maximum moment obtained from full scale bending tests. Once η is obtained, the ultimate horizontal shear strength, τ_u, can be calculated using Eq. 4.11 and after applying some reduction and safety factors (ECCS, 1998) the value is used for designing other slabs made of steel deck similar to the tested deck. It can be seen from Fig. 4.2(a) that in this procedure, τ_u is directly affected by the maximum moment. This method of determining the horizontal shear strength has two major sources of inaccuracies. The first was identified in the previous section where the maximum moment can vary but the variation of the shear bond strength does not necessarily follow the moment magnitude. For example, if the shear span is held constant, increasing the slab thickness will increase the moment capacity but this does not change the shear bond strength accordingly.

The other source of inaccuracy is that the effect of slenderness is not properly addressed when η is determined. For a given deck, tests on compact specimens produce higher shear strength than tests conducted on slender slabs (refer to Table 4.3 and discussion in Sec. 4.7.2). This indicates that if the shear strength obtained from a compact slab that was used to design a slender slab, an unsafe result is produced. Likewise if the compact slab was designed based on the shear strength obtained from slender slab, an overly conservative result may occur.

Clause 10.3.1.2 of Eurocode 4 (1994) provides a guide for the test specimens where the thickness and the span should be varied to represent the whole range of shear connections and at least three tests having a value for η between 0.7 and 1.0. However from the experiments, and as revealed by the plots of η versus d/L_s in Fig. 6.13, the recommended value of η between 0.7 and 1.0 is difficult to achieve.

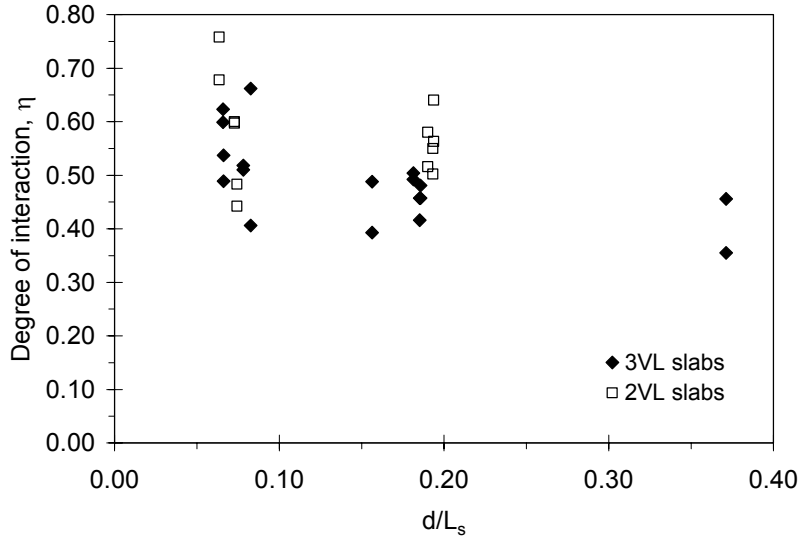

Fig. 6.13 Degree of interaction versus compactness from small scale tests.

Despite specifying the whole range of shear connection, ECCS (1998) always suggests to use the smallest values for τ_u, which can be found from the high values of η ($\eta \approx 1.0$). This means the minimum value of τ_u is obtainable from region A of Fig. 4.1, which is the region for slender specimens. This provision parallels the requirement set forth in the draft copy of Eurocode 4 (2001). The new specification specifies that the test series for determining the τ_u should be carried out on the slenderest specimen possible while still providing failure in longitudinal shear. If this provision is followed, then the design results are always too conservative for the slabs more compact than the test specimens. This

procedure results in the PSC method being less accurate than the *m-k* method if it is used over a wide range of slab geometry. Furthermore, there is no specific detail for streamlining the test results to gain benefit from the tests with variable thickness and shear spans, as suggested in the Eurocode 4 (1994) test procedure.

6.5.2 Proposed improvement

Given that the shear bond strength varies with the compactness of the slab, a single value of τ_u cannot represent the whole range of slab slenderness. The solution is to conduct tests on specimens with variable slenderness, similar to those of the *m-k* test requirement (Fig. 4.1) and do interpolation to obtain value for τ_u for different slenderness slab using the shear bond-slenderness equation (Eq. 6.9). The calculation of η and τ_u for each data point can follow either the PSC method as present in Sec. 4.5 or the force equilibrium method set forth in Sec. 4.6.2. Because Eq. 6.9 is a linear equation, only two regions of tests are needed to represent the whole range of slab slenderness just as for the *m-k* method. The application of shear bond-slenderness equation is demonstrated below.

In this exercise the ultimate shear bond stress, τ_u, for small scale specimen 3VL16-4-7.5 and 3VL16-14-5 were first determined according to the PSC method (Eq. 4.4 to 4.11 and Fig. 4.2a) and the values are shown in Table 6.1. Data from these specimens are then plotted in Fig. 6.14 from which the *p* and *s* values are obtained by regression analysis. With these parameters, the τ_u values for other 3VL slabs are obtained from interpolation. Once τ_u values for the corresponding slabs are obtained, the design loads for other 3VL slabs are calculated according to Eq. 4.13 to 4.18 as shown graphically by Fig. 4.3. A partial safety factor of 1.0 is used in this exercise. The same procedure was repeated for 2VL slabs where test data of specimens 2VL20-7-6.5 and 2VL20-9-4, which are also shown in Table 6.1,

were used to obtain the regression line for the shear bond stress as shown in Fig. 6.15. For comparison, the ultimate load calculations according to the *m-k* method (Eq. 4.3) using data from the same specimens were also performed and the values are shown in Table 6.2. The results from both methods are compared with small and full scale test data by specifying the ratio of test-to-calculated values and they are tabulated in Table 6.3 and Table 6.4 respectively. Graphical comparisons are depicted in Fig. 6.16 and Fig. 6.17.

For the PSC method, the mean of the ratios of small scale test-to-calculated values is 1.08 with a 10% average variation of the test values from the calculated values as indicated by the standard deviation of 0.10. For the *m-k* method the same comparison of the ratio give 1.13 and 0.11 for the mean and standard deviation, respectively. Comparison between the ratios of full scale test-to-calculated values according to the PSC method results in 1.07 for the mean and 0.17 for the standard deviation. The same comparison for the *m-k* method gives 1.11 and 0.12 for the mean and standard deviation respectively. Both methods are relatively conservative compared to the full scale test results in the compact region and comparable in the slender region.

This exercise has demonstrated that the ultimate loads calculated using the PSC method employing the shear bond-slenderness equation are similar in accuracy to those calculated with the *m-k* method. This implies that the PSC method was greatly improved. It can be used to design slabs of variable slenderness accurately using only two sets of test data. The direct comparison between the PSC and the *m-k* methods is now possible because the shear bond-slenderness equation used in the PSC method employs the concept of linear interpolation similar to the *m-k* equation. Such comparison is depicted in Fig. 6.18.

Table 6.1 Design parameters according to the PSC method

Specimen ID	Test	Max. M_{test} (lb-ft)	M_{pRm} (lb-ft)	η	τ (psi)	t (in.)	d (in.)	$L_{s\ (clear)}$ (in.)	p	s
3VL16-4-7.5	A	169	282.84	0.456	86.98	0.0598	5.940	12	14055	43.32
	B	147	282.84	0.355	67.68	0.0598	5.940	12		
3VL16-14-5	A	114	154.04	0.489	28.69	0.0598	3.440	48		
	B	118	154.04	0.537	31.51	0.0598	3.440	48		
2VL20-7-6.5	A	97	144.96	0.580	38.57	0.0358	5.323	24	26158	-13.78
	B	89	144.96	0.516	34.29	0.0358	5.323	24		
2VL20-9-4	A	50	73.38	0.483	23.66	0.0358	2.823	34		
	B	48	73.38	0.442	21.66	0.0358	2.823	34		

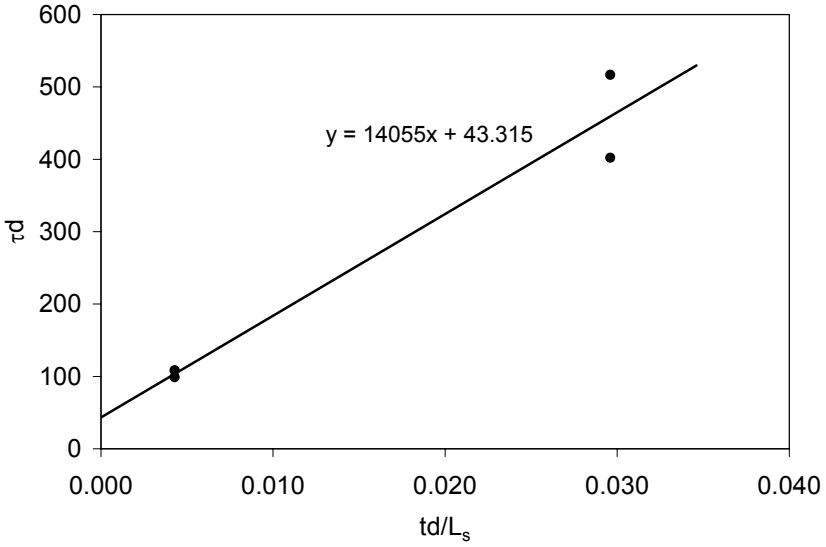

Fig. 6.14 Shear bond-slenderness equation plot for 3VL16-4-7.5 and 3VL16-14-5

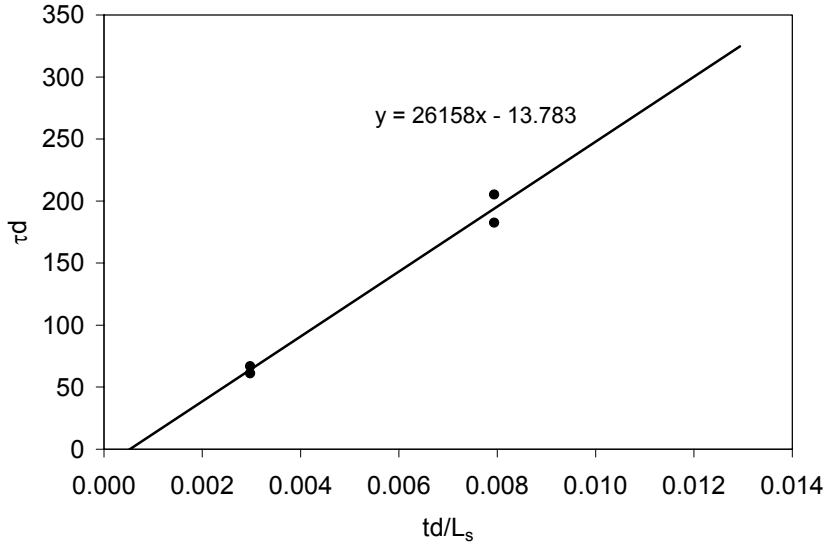

Fig. 6.15 Shear bond-slenderness equation plot for 2VL20-7-6.5 and 2VL20-9-4

Table 6.2 Design parameters according to the *m-k* method (Eurocode 4)

Specimen ID	Test	Max. V_{test} (lb)	b	L_s (clear)	A_p	d	$\frac{A_p}{bL_s}$	$\frac{V_{test}}{bd}$	m	k
3VL16-4-7.5	A	10590	12	12	0.993	5.940	0.0069	148.5	16341	25.99
	B	9180	12	12	0.993	5.940	0.0069	128.8		
3VL16-14-5	A	2200	12	48	0.993	3.440	0.0017	53.2		
	B	2280	12	48	0.993	3.440	0.0017	55.2		
2VL20-7-6.5	A	3450	12	24	0.546	5.323	0.0019	54.0	24236	5.84
	B	3170	12	24	0.546	5.323	0.0019	49.6		
2VL20-9-4	A	1320	12	34	0.546	2.823	0.0013	39.1		
	B	1270	12	34	0.546	2.823	0.0013	37.5		

Table 6.3 Results of the PSC method using Eq. 6.9 and the *m-k* method using Eq. 4.3 and comparison with the small scale test data

Specimen ID	Test	Ult. load by PSC method, W_{uPSC} (psf)	Ult. load by *m-k* method, W_{um-k} (psf)	Ult. load from small scale test, W_{us} (psf)	W_{us} / W_{uPSC}	W_{us} / W_{um-k}
3VL20-8-7.5	A	1170	1327	1390	1.19	1.05
	B	1170	1327	1370	1.17	1.03
3VL20-11-5	A	485	432	510	1.05	1.18
	B	485	432	410	0.85	0.95
3VL18-8-7.5	A	1440	1586	1490	1.03	0.94
	B	1440	1586	1570	1.09	0.99
3VL18-13-5	A	415	418	410	0.99	0.98
	B	415	418	420	1.01	1.00
3VL16-4-7.5	A	7350	7118	10170	1.38	1.43
	B	7350	7118	8820	1.20	1.24
3VL16-8-7.5	A	1800	1838	2100	1.17	1.14
	B	1800	1838	2160	1.20	1.18
3VL16-10-7.5	A	1210	1220	1350	1.12	1.11
	B	1210	1220	1190	0.98	0.98
3VL16-12-5	A	610	513	610	1.00	1.19
	B	610	513	610	1.00	1.19
3VL16-14-5	A	455	402	430	0.95	1.07
	B	455	402	440	0.97	1.09
2VL20-7-6.5	A	1370	1320	1600	1.17	1.21
	B	1370	1320	1480	1.08	1.12
2VL20-9-4	A	445	423	480	1.08	1.13
	B	445	423	460	1.03	1.09
2VL18-7-6.5	A	1840	1728	1830	0.99	1.06
	B	1840	1728	1950	1.06	1.13
2VL18-11-4	A	417	364	450	1.08	1.23
	B	417	364	450	1.08	1.23
2VL16-7-6.5	A	2300	2144	2620	1.14	1.22
	B	2300	2144	2390	1.04	1.11
2VL16-12-4	A	430	380	470	1.09	1.24
	B	430	380	500	1.16	1.32
				Mean	1.08	1.13
				Standard deviation	0.10	0.11

Table 6.4 Results of the PSC method using Eq. 6.9 and the *m-k* method using Eq. 4.3 and comparison with the full scale test data

Specimen ID	Test	Ult. load by PSC method, W_{uPSC} (psf)	Ult. load by *m-k* method, W_{um-k} (psf)	Ult. load from full scale test, W_{uf} (psf)	W_{uf} / W_{uPSC}	W_{uf} / W_{um-k}
3VL20-8-7.5	A	1170	1327	1670	1.43	1.26
	B	1170	1327	1650	1.41	1.24
3VL20-11-5	A	485	432	420	0.87	0.97
	B	485	432	450	0.93	1.04
3VL18-8-7.5	A	1440	1586	1790	1.24	1.13
	B	1440	1586	1840	1.28	1.16
3VL18-13-5	A	415	418	390	0.94	0.93
	B	415	418	390	0.94	0.93
3VL16-4-7.5	A	7350	7118	-	-	-
	B	7350	7118	-	-	-
3VL16-8-7.5	A	1800	1838	2140	1.19	1.16
	B	1800	1838	2230	1.24	1.21
3VL16-10-7.5	A	1210	1220	-	-	-
	B	1210	1220	-	-	-
3VL16-12-5	A	610	513	-	-	-
	B	610	513	-	-	-
3VL16-14-5	A	455	402	380	0.84	0.94
	B	455	402	410	0.90	1.02
2VL20-7-6.5	A	1370	1320	1540	1.12	1.17
	B	1370	1320	1460	1.07	1.11
2VL20-9-4	A	445	423	460	1.03	1.09
	B	445	423	480	1.08	1.13
2VL18-7-6.5	A	1840	1728	1940	1.05	1.12
	B	1840	1728	1790	0.97	1.04
2VL18-11-4	A	417	364	430	1.03	1.18
	B	417	364	470	1.13	1.29
2VL16-7-6.5	A	2300	2144	1860	0.81	0.87
	B	2300	2144	2380	1.03	1.11
2VL16-12-4	A	430	380	480	1.12	1.26
	B	430	380	470	1.09	1.24
				Mean	1.07	1.11
				Standard deviation	0.17	0.12

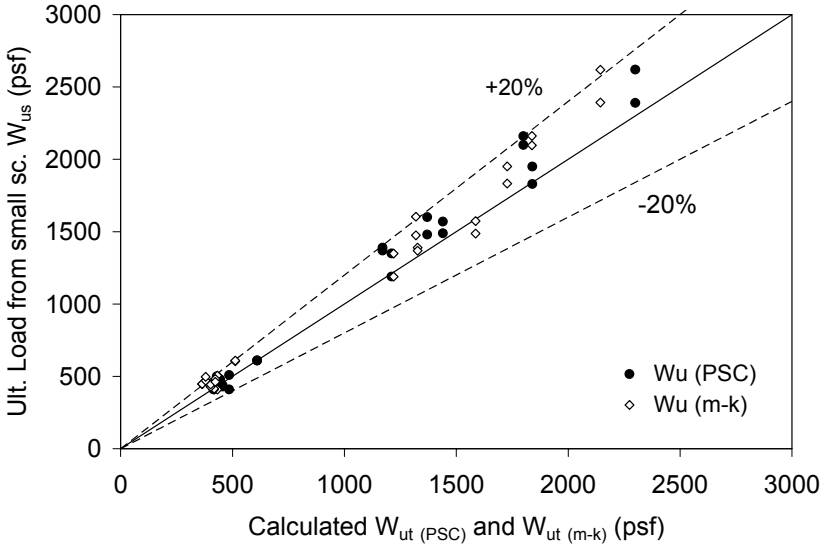

Fig. 6.16 Comparison between ultimate loads from small scale tests and the calculated load using the *PSC* and *m-k* methods (data from Table 6.3).

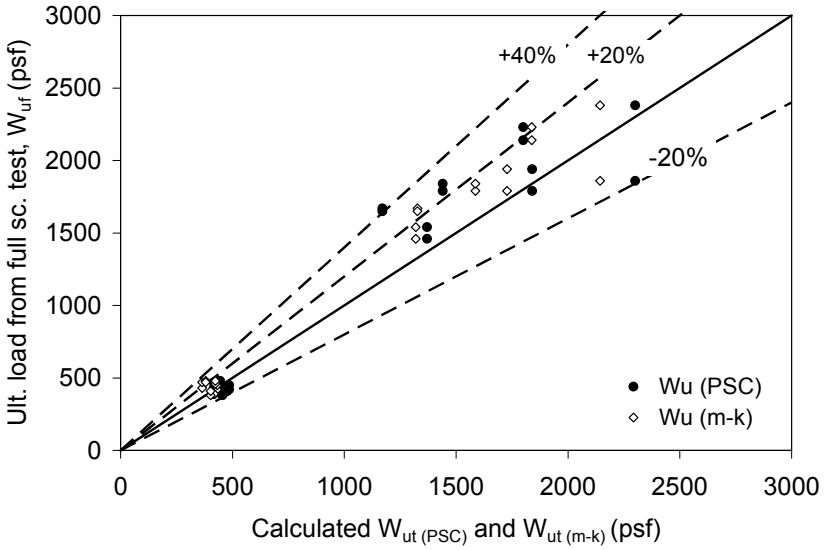

Fig. 6.17 Comparison between ultimate loads from full scale tests and the calculated loads using the PSC and *m-k* methods (data from Table 6.4).

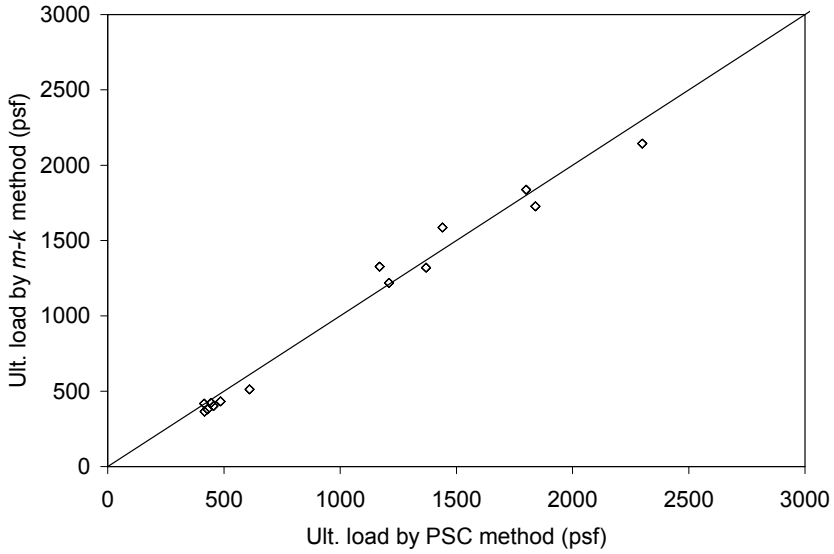

Fig. 6.18 Comparison between loads calculated using the *m-k* and the PSC methods

6.6 Effect of slenderness on the *PSC* and *m-k* method

It has been shown that slenderness is a parameter that influences the strength of a slab. Test and analysis results as depicted in Fig. 3.15 and Fig. 6.10 confirmed this behavior. In the previous section the PSC and the *m-k* methods are slightly conservative when compared with the test data for compact slabs but were in the same range for the slender slabs. In this section, the PSC and the *m-k* methods are compared with the test and FE results to determine the accuracy of both PSC and *m-k* methods when dealing with variable slenderness.

Results of the FE analysis in Sec. 6.3.4 for models 3VL16, 3VL18 and 2VL20 with variable slenderness were analyzed using the PSC and the *m-k* methods. Linear regression was applied to the FE results to obtain the values for *m*, *k*, *p* and *s*. The results in the form of support reactions are plotted against the slenderness as shown in Fig. 6.19, Fig. 6.20 and

Fig. 6.21 for model 3VL16, 3VL18 and 2VL20 respectively. All data series are fitted with power function curves.

It can be observed from the figures that the PSC method is accurate at large slenderness values but started to decrease in accuracy as compared to the test data (Fig. 6.19) and other methods (Fig. 6.19, 6.20 and 6.21) as the slenderness reduces below 7.0. The difference is as large as 40% for a slenderness value of 2.0. The differences are within 20% for slenderness values of 4.0 or greater.

The conservativeness of the PSC method for compact slabs can be attributed to the mechanical model of the method which does not recognize the effect of direct load transfer to the support, the effect of increased clamping of concrete to the deck, deep beam behavior and other factors associated with high compactness. An example is depicted in Fig. 6.22 that shows how different load positions such as moving from point 1 to point 2, would result in direct load transfer to the support. This effect was captured in the FE model. Despite the same linear interpolation, the *m-k* method correlates more closely to the FE results (and the test results for models 3VL16) compared to the PSC method. This can be attributed to the *m-k* equation which interpolates directly from maximum load and does not depend on the mechanical model as opposed to the PSC method which interpolates the shear bond stress and depends on the mechanical model.

Even though the PSC method is conservative for a slab that is very compact, it is insignificant in terms of application in design because the span and thickness of the slab at this slenderness is not practicable in actual construction. For the normal range, the accuracy is well within 10%. To reduce the scatter of the results, the test specimens should be as compact as possible for one region and as slender as possible for the other region.

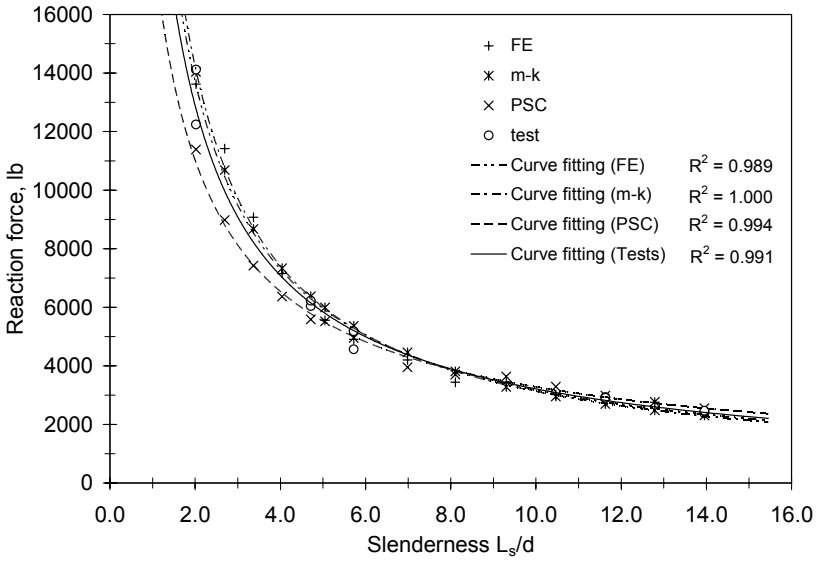

Fig. 6.19 Analysis results for 3VL16 slabs with variable compactness

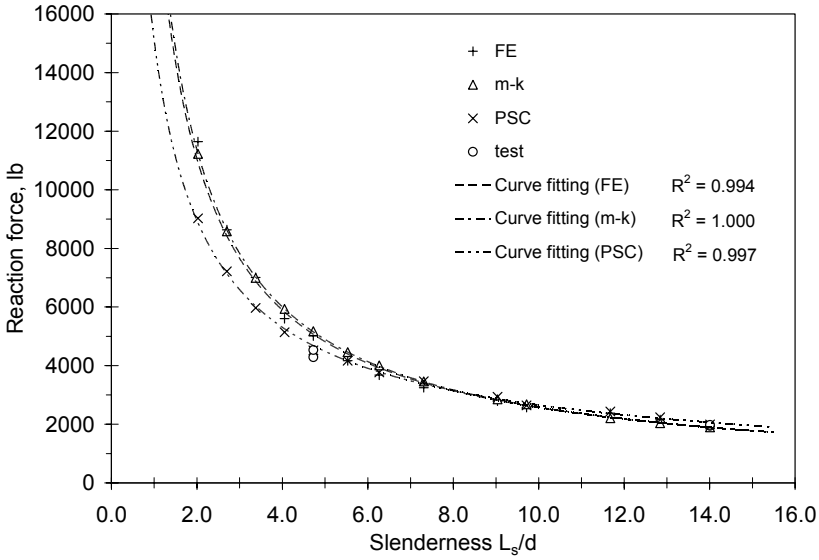

Fig. 6.20 Analysis results for 3VL18 slabs with variable compactness

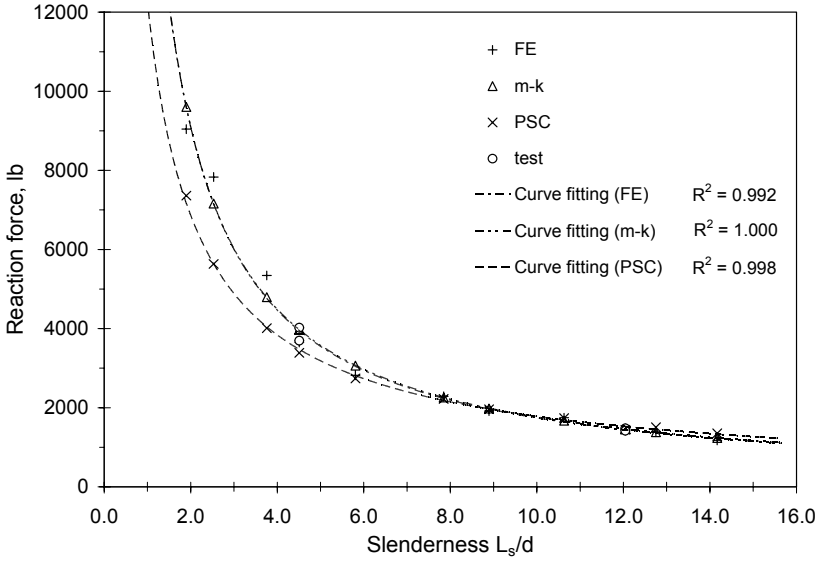

Fig. 6.21 Analysis results for 2VL20 slabs with variable compactness

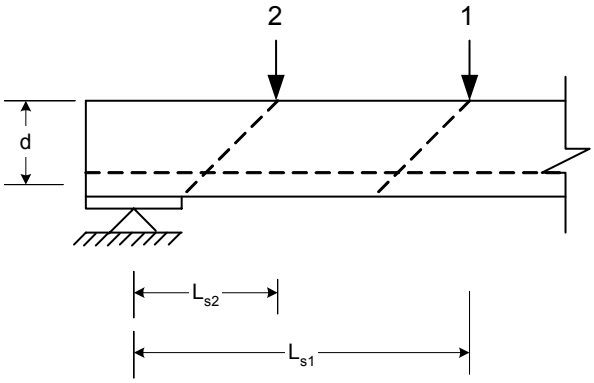

Fig. 6.22 Slenderness, L_s/d , which is determined by load position can influence the slab strength

6.7 Concluding remarks

1) The maximum shear bond stress varies linearly with slab compactness where the values are larger for compact slabs and smaller for slender slabs. An equation that expresses this relation was derived and is called the shear bond-slenderness equation.

2) The shear bond stress-slip curve also varies linearly with the slab slenderness. To obtain accurate modeling, the shear bond stress property should be adjusted according to the slab slenderness and this can be done by linear interpolation from two known curves.

3) The slenderness effect was introduced into the PSC method using shear bond-slenderness equation. The method was improved significantly compared to the present procedure which does not consider slenderness at all. The PSC method can now be used with greater accuracy to design slabs whose dimensions are different from the tested specimen.

4) The PSC method is accurate at large slenderness, but becomes conservative when the slenderness is reduced. The reason is that the PSC method is unable to recognize the effects associated with increasing compactness. The conservativeness of the PSC method can be kept within 10% by limiting the slenderness to 4.0.

5) The shear bond-slenderness equation contains steel deck thickness as a parameter and the small scale test data fitted well into this equation. With the presence of the deck thickness, the required number of lab tests for use in this equation can be reduced, in which no new series of tests is needed for

slabs with different deck thickness. This is in agreement with the findings of Seleim and Schuster (1985) and the procedure used in the CSSBI (1996) specification.

7 Conclusions and recommendations

7.1 Conclusions

A new type of small scale composite slab test was successfully developed. The test performance was comparable with the full scale test in predicting composite slab strength and behavior. The small scale specimen is very easy and simple to build and test with a simple test apparatus, inexpensive and reusable forms, angle straps and C-clamps to strengthen the edge webs. With the small scale tests, four times as much data as full scale tests for the same materials, effort and floor area can be gathered.

The small scale test developed in this research can be used for performance evaluation and can also provide data for use in present design methods, namely the *m*-*k* and the PSC methods, as well as for determining the shear bond property for modeling the slab in the finite element method. The same test can also be employed in the development of a new type of embossment and deck profile, thus eliminating the need for the elemental push off test. Because of its small scale nature, multi-purpose and simplicity to conduct, the test is certainly very economical and should be considered a replacement for the full scale test recommended in the current design specifications.

In an attempt to determine the shear bond stress property from the small scale test for numerical modeling purposes, two calculation methods were introduced, namely the work method and the force equilibrium method. The results of the work method were

found to be too conservative for most compact slabs. On the other hand the force equilibrium method was more accurate given that its maximum stress value compared well with the existing PSC method.

Because the small scale test is a bending type test, it inherits the characteristics of actual slab bending. As a result, the shear bond property derived out of the test data has implicitly included all affects associated with slab bending, namely the effects of vertical separation, frictional resistance at supports, reduction of shear resistance due to high strain in the deck and the clamping of concrete to the deck due to bending curvature and profile shape. This renders the shear bond property more representative of a real slab than the property obtained from traditional push tests. Thus the small scale test developed here is more favorable than the push off type tests for shear bond data gathering.

It has been shown that the FE analysis using a smeared crack model available in ABAQUS/Explicit employing the shear bond stress property derived from the small scale bending test can be accomplished successfully without a need to incorporate those parameters (support friction, vertical separation and high strain effect) into the model, thus simplifying the FE model.

Test results showed that the shear bond stress varied linearly with the slab compactness. A shear bond-slenderness equation was successfully derived to express this relationship. Because of this variation the shear bond stress property used in the numerical model should be adjusted according to the compactness of the models so that accurate analysis results can be obtained. The adjustment can be done by linear interpolation based on two series of known data.

Finite element analysis utilizing an invariable shear bond stress property might produce good results for a particular geometry and slenderness but might be erroneous for other models with different slenderness. Hence any analytical method that is derived from finite element analysis utilizing invariable shear bond stress-slip property should be used with caution.

The shear bond-slenderness equation was also implemented successfully to account for the effect of the slenderness in the PSC method. Using this equation, the PSC method was improved significantly, especially for estimating the shear bond strength of slabs of variable dimensions, thus enabling the PSC method to be compared vis-à-vis with the *m-k* method. The shear bond-slenderness equation also provided a means for expressing the behavior relating the shear bond stress with the slab thickness. It was found that the shear bond stress only changed marginally when the slab thickness was changed. The change can be ignored for modeling purposes.

Pertaining to the slenderness effect, the accuracy of the PSC method utilizing the shear bond-slenderness equation was compared to the *m-k* method using the finite element method and the test results. The *m-k* method correlated well with the FE and the test results for all slenderness. On the other hand the PSC method was accurate for slender slabs but conservative for the compact ones. However this conservativeness can be considered insignificant because the highly compact slabs are impractical and most probably will not be used in normal construction practice. The slenderness limit was also proposed to indicate the point where the PSC method started to differ significantly from the FE and the test results.

Because the shear bond stress varies linearly with the slab compactness, only two regions of small scale tests are required to provide adequate data for design with the PSC method. This is similar to test requirement for the *m-k* method and therefore data from the same test can be used for both methods. The same number of specimens and test procedure as prescribed in the present specifications for conducting full scale tests can be followed.

7.2 Recommendations

The PSC design method is a good mechanical model for design of composite slabs. It is based on a clear mechanical model, analytically simple and easy to implement, and does not involve complicated numerical analysis. With the introduction of shear bond-slenderness equation, the PSC method has been significantly improved and compares well with the *m-k* method. With its advantage of having clear mechanical model, plus the economic benefit that can be derived by employing small scale tests such as the type proposed in this research, the versatility of the PSC method cannot be over emphasized. It is recommended that the PSC method be employed in the new addition of the ASCE standard as an alternative to the *m-k* method.

It is recommended also that the *p* and *s* value (i.e. the slope and intercept of the *shear-bond slenderness* line) for the most common profiles to be stated in the specification so that engineers can conduct analysis and design as needed rather than only selecting values from a manufacturer's load table. To achieve this objective cooperation and sponsorship from deck manufacturers that will benefit from their product being specified in the specification is needed.

Design of composite slabs can now be conducted at a much cheaper cost by employing the small scale tests such as the type proposed in this research. Because of cost

benefit, and its ability to produce results as good as those from full scale specimens, it is also recommended that the small scale test be included in the ASCE standard.

Application of the small scale test should not be limited to the trapezoidal profile only. As continuing work, the small scale test research should be conducted on slabs using other types of profiles and details. This includes slabs utilizing re-entrant shapes and deep deck profiles, slabs with other types of construction details such as shear studs at the slab ends, slabs that contain additional positive reinforcement, and continuous slabs with negative reinforcement at intermediate supports.

Other recommended future research includes testing of small scale specimens using air bag or vacuum chamber for uniform loading, and modeling of the vertical separation between the concrete and the steel deck and its impact on the shear bond resistance.

References

Abaqus Online Documentation, Version 6.3-1 (2002). Hibbitt, Karlsson and Sorenson Inc. Pawtucket, R.I.

Airumyan, E., Belyaev, V., and Rumyancev, I. (1990). "Efficient Embossment for Corrugated Steel Sheeting." *IABSE Symposium on Mixed Structures Including New Materials*, Brussels, Belgium, 137-142.

Alfaiate, J., Pires, E. B., and Martins, J. A. C. (1997). "A Finite Element Analysis of Non-Prescribed Cracks Propagtion in Concrete." *Computers & Structures*, 63(1), 17-26.

An, L. (1993). "Load Bearing Capacity and Behaviour of Composite Slabs with Profiled Steel Sheet," Phd Dessertation, Chalmers University of Technology, Sweden.

An, L., and Cederwall, K. (1992). "Composite Slabs Analysed by Block Bending Test." *Proceedings of the 11th International Specialty Conference on Cold-Formed Steel Structures*, University of Missouri-Rolla, 268-282.

ASCE. (1992). *Standard for the Sturctural Design of Composite Slabs. ANSI/AASCE 3-91*, American Society of Civil Engineers, New York.

Bode, H., and Dauwel, T. (1999). "Steel-Concrete Composite Slabs - Design Based on Partial Connection." *Proceedings of the International Conference on Steel and Composite Structures*, Delft, The Netherlands, 2.1-2.10.

Bode, H., Minas, F., and Sauerborn, I. (1996). "Partial Connection Design of Composite Slabs." *Structural Engineering International* (1(Jan.)), 53-56.

Bode, H., and Sauerborn, I. (1992). "Modern Design Concept for Composite Slabs with Ductile Behaviour." *Proceedings of an Engineering Foundation Conference on Composite Construction in Steel and Concrete II*, American Society of Civil Engineers, 125-141.

BS-5950. (1994). *Structural Use of Steelwork in Building - Part 4: Code of Practice for Design of Composite Slabs with Profiled Steel Sheeting*, British Standard Institution, London.

Burnet, M. (1998). "Analysis of Composite Steel and Concrete Flexural Members that Exhibit Partial Shear Connection," PHD Thesis, University of Adelaide, Australia.

Calixto, J. M., Lavall, A. C., Melo, C. B., Pimenta, R. J., and Monteiro, R. C. (1998). "Behaviour and Strength of Composite Slabs with Ribbed Decking." *J. Construct. Steel Res.*, 46(1-3), Paper 110.

Crisinel, M., and Marimon, F. (2003). "A New Simplified Method for the Design of Composite Slabs." *J. Construct. Steel Res.*, 60(3-5), 481-491.

CSSBI. (1996). *Standard for Composite Steel Deck, CSSBI 12M - 96*, Canadian Sheet Steel Building Institute.

Daniels, B. J. (1988). "Shear Bond Pull-out Tests for Cold-Formed-Steel Composite Slabs." ICOM - Construction Metallique, Department de Genie Civil, Ecole Polytechnique Federale de Lausanne.

Daniels, B. J., and Crisinel, M. (1993a). "Composite Slab Behavior and Strength Analysis. Part I: Calculation Procedure." *Journal of Structural Engineering,* 119(1-4), 16-35.

Daniels, B. J.. and Crisinel, M. (1993b). "Composite Slab Behavior and Strength Analysis. Part II: Comparisons With Test Results And Parametric Analysis." *Journal of Structural Engineering,* 119(1-4), 36-49.

Easterling, W. S., and Young, C., S. (1992). "Strength of Composite Slabs." *Journal of Structural Engineering*, 118(9), 2370-2389.

ECCS. (1995). "Design Manual for Composite Slabs." *Report No. 87*, European Convention for Constructional Steelwork, Brussels, Belgium.

ECCS. (1998). "Longitudinal Shear Resistance of Composite Slabs: Evaluation of Existing Tests." *Report No. 106*, European Convention for Constructional Steelwork, Brussels, Belgium.

Eurocode 4. (1994). *Design of Composite Steel and Concrete Structures, Part 1.1, General Rules and Rules for Buildings. ENV 1994-1-1:1992*, European Committee for Standardization, Brussels.

Eurocode 4. (2001). *Design of Composite Steel and Concrete Structures - Part 1.1: General Rule and Rules for Buildings, EN 1994-1.1:2001, Draft No. 3*, European Committee for Standardization, Brussels.

Evans, H. R., and Wright, H. D. (1988). "Steel-Concrete Composite Flooring Deck Structures." *Steel-Concrete Composite Structures, Stability and Strength,* Narayanan, R., ed., Elsevier, London, 21-52.

Heagler, R. B., Luttrell, L. D., and Earterling, W. S. (1991). *Composite Deck Design Handbook*, Steel Deck Institute, Canton, Ohio.

Hillerborg, A., Modeer, M., and Peterson, P. E. (1976). "Analysis of Crack Formation and Crack Growth in Concrete by Means of Fracture Mechanics and Finite Elements." *Cement and Concete Research*, 6, 773-782.

Johnson, R. P. (1994). *Composite Structures of Steel and Concrete, Vol. 1: Beams, Slabs, Columns, and Frames for Buildings*, Blackwell Scientific Publication, Oxford.

Jolly, C. K., and Zubair, A. K. (1987). "The Efficiency of Shear-Bond Interlock between Profiled Steel Sheeting and Concrete." *Proceedings of the International Conference on Steel and Aluminum Structures Composite Steel Structures, Advances, Design and Construction*, Cardiff, 127-136.

Luttrell, L. D. (1986). "Methods for Predicting Strength in Composite Slabs." *Proceedings of the 8th International Specialty Conference on Cold-Formed Steel Structure*, St. Louis Missouri, 419-431.

Luttrell, L. D. (1987). "Flexural Strength of Composite Slabs." *Composite Steel Structures - Advances, Design and Construction,* Narayanan, R., Ed., Elsevier, London, 106-115.

Luttrell, L. D., and Davidson, J. H. (1973). "Composite Slabs with Steel Deck Panels." *Proceedings of the 2nd International Specialty Conference on Cold-Formed Steel Structures*, St. Louis, Missouri, 573-603.

Luttrell, L. D., and Prasannan, S. (1984). "Strength Formulations for Composite Slabs." *Proceedings of the 7th International Specialty Conference on Cold-Formed Steel Structures*, St. Louis, Missouri, 307-324.

Patrick, M. (1990). "A New Partial Shear Connection Strength Model for Steel Construction Composite." *Journal of the Australian Institute of Steel Construction*, 24(3), 2-17.

Patrick, M., and Bridge, R. Q. (1992). "Design of Composite Slabs for Vertical Shear." *Proceedings of an Engineering Foundation Conference on Composite Construction in Steel and Concrete II*, American Society of Civil Engineer, 304-322.

Patrick, M., and Bridge, R. Q. (1994). "Partial Shear Connection Design of Composite Slabs." *Engineering Structures*, 16(5), 348-362.

Patrick, M., and Poh, K. W. (1990). "Controlled Test for Composite Slab Design Parameters." *IABSE Symposium, Brussels, Belgium - Mixed Structures, Including New Materials*, Zurich, Switzerland, 227-231.

Plooksawasdi, S. (1977). "Evaluation and Design Formulations for Composite Steel Deck," Phd Dissertation, West Virginia University, Morgantown, West Virginia.

Porter, M., Ekberg, C. E., Greimann, L. F., and Elleby, H. A. (1976). "Shear-Bond Analysis of Steel-Deck-Reinforced Slabs." *Journal of the Structural Division*, 102(ST12), 2255-68.

Porter, M. L., and Ekberg, C.E. (1978). "Compendium of ISU Research Conducted on Cold-Formed Steel Deck-Reinforced Slab Systems." Engineering Research Institute, Iowa State University, Ames, Iowa.

Porter, M. L., and Ekberg, C. E. (1971). "Investigation of Cold Formed Steel Deck Reinforced Concrete Floor Slabs." *Proceedings of the 1st International Specialty Conference on Cold-Formed Steel Structures*, Missouri, Rolla, 79-185.

Porter, M. L., and Ekberg, C. E. (1975a). "Design Recommendations for Steel Deck Floor Slabs." *Proceedings of the 3rd International Specialty Conference on Cold-Formed Steel Structures*, St. Louis Missouri, 761-785.

Porter, M. L., and Ekberg, C. E. (1975b). "Design Vs. Test Results for Steel Deck Floor Slabs." *Proceedings of the 3rd International Specialty Conference on Cold-Formed Steel Structures*, St. Louis Missouri, 793-809.

Porter, M. L., and Ekberg, C. E. (1976). "Design Recommendation for Steel Deck Floor Slab." *Journal of the Structural Division*, 102(ST11), 2121-2136.

Prasannan, S. (1983). "Flexural Response of Composite Steel-Deck Slab Systems," MSc. Thesis, West Virginia University, Morgantown, West Virginia.

Schumacher, A., Laane, A., and Crisinel, M. (2000). "Development of a New Design Approach for Composite Slabs." *Proceedings of an Engineering Foundation Conference on Composite Construction in Steel and Concrete IV*, American Society of Civil Engineers, 1-12

Schuster, R. M. (1970). "Strength and Behavior of Cold-Rolled Steel-Deck-Reinforced Concrete Floor Slabs," Phd Dissertation, Iowa State University, Ames, Iowa.

Seleim, S. S. (1979). "Ultimate Shear-Bond Capacity of Composite Steel Deck Concrete Slabs.," MSc. Thesis, University of Waterloo, Ontario, Canada.

Seleim, S. S., and Schuster, R. M. (1985). "Shear-Bond Resistance of Composite Deck-Slabs." *Canadian Journal of Civil Engineering*, 12(316-323).

Shen, G. (2001). "Performance Evaluation of New Corrugated-Type Embossments for Composite Deck," MSc. Thesis, Virginia Polytechnic Institute and State University, Blacksburg, Virginia.

Stark, J. (1978). "Design of Composite Floors with Profiled Steel Sheet." *Proceedings of the 4th International Specialty Conference on Cold-Formed Steel Structures,* St. Louis Missouri-Rolla, 893-992

Stark, J. W., and Brekelmans, J. W. (1990). "Plastic Design of Continuous Composite Slabs." *J. Construct. Steel Res.*, 15(1-2), 23-47.

Tenhovuori, A., and Leskela, M. V. (1997). "Various Tests for Defining the Behaviour of Composite Slabs." *IABSE International Conference in Composite Construction, Conventional and Innovative*, Zurich, 543-548.

Tenhovuori, A., and Leskela, M. V. (1998). "Longitudinal Shear Resistance of Composite Slabs." *J. Construct. Steel Res.*, 46(1-3), Paper 319.

Tenhovuori, A., Karkkainen, K., and Kanerva, P. (1996). "Parameters and Definitions for Classifying the Behaviour of Composite Slabs." *Proceeding of an Engineering Foundation Conference on Composite Construction in Steel and Concrete III,* American Society of Civil Engineers, 752-764.

Terry, A. S., and Earterling, W. S. (1994). "The Effect of Typical Construction Details on the Strength of Composite Slabs." *Report No. CE/VPI-ST 94/05*, Department of Civil Engineering, Virginia Polytechnic Institute and State University, Blacksburg.

Tremblay, R., Rogers, C. A., Gignac, P., and Degrange, G. (2002). "Variables Effecting the Shear-Bond Resistance of Composite Floor Deck Systems." *Proceedings of the 16th International Specialty Conference on Cold-Formed Steel Structures*, Orlando, Florida, 663-676.

Veljkovic, M. (1993). "Development of a New Sheeting Profile for Composite Floors: Experimental Study And Interpretation." *Research Report Tulea 1993:47*, Lulea University of Technology.

Veljkovic, M. (1994). "Interaction between Concrete and Sheeting in Composite Slabs." *S-971 87 LULEA*, Lulea University of Technology, Division of Steel Structures, Lulea, Sweden.

Veljkovic, M. (1995). "Longitudinal Shear Capacity of Composite Slabs." *Nordic Steel Construction Conference '95*, Malmo, Sweden.

Veljkovic, M. (1996a). "Behaviour and Resistance of Composite Slabs," Phd Thesis, Lulea University of Technology, Lulea, Sweden.

Veljkovic, M. (1996b). "An Improved Partial Connection Method for Composite Slab Design." *Proceedings of an Engineering Foundation Conference in Composite construction in steel and concrete III,* American Society of Civil Engineers, 644-659.

Veljkovic, M. (1998). "Influence of Load Arrangement on Composite Slab Behaviour and Recommendations for Design." *J. Construct. Steel Res.*, 45(2), 149-178.

Veljkovic, M. (2000). "Behaviour and Design of Shallow Composite Slab." *Engineering Foundation Conference - Composite Construction IV*, Banff, Alberta, Canada.

Widjaja, B. R. (1997). "Analysis and Design of Steel Deck-Concrete Composite Slabs," Phd Dissertation, Virginia Polytechnic Institute and State University, Blacksburg.

Widjaja, B. R., and Easterling, W. S. (1996). "Strength and Stiffness Calculation Procedures for Composite Slabs." *Proceedings of the 13th International Specialty Conference on Cold-Formed Steel Structures*, St. Louis Missouri, 389-401.

Wright, H. D., and Evans, H. R. (1987). "Observations on the Design and Testing of Composite Floor Slabs." *Steel Construction Today*, 1, 91-99.

Wright, H. D., and Evans, H. R. (1990). "A Review of Composite Slab Design." *Proceedings of the 10th International Specialty Conference on Cold-Formed Steel Structures*, St. Louis Missouri, 27-47.

Wright, H. D., and Veljkovic, M. (1996). "Towards a Numerical Procedure for Composite Slab Assessment." *Proceedings of the 13th International Specialty Conference on Cold-Formed Steel Structures*, St. Louis, Missouri, U.S.A

Zubair, A. K. M. (1989). "Improvement of Shear-Bond in Composite Steel and Concrete Floor Slabs," Phd Thesis, University of Southampton.